NTNU

Norwegian University of
Science and Technology

Removal of Phosphorus from Silicon Melts by Vacuum Refining

Buhle Sinaye Xakalashe

Silicon and Ferroalloy Production

Submission date: August 2011

Supervisor: Merete Tangstad, IMTE

Norwegian University of Science and Technology
Department of Materials Science and Engineering

Removal of Phosphorus from Silicon Melts by Vacuum Refining

Buhle Sinaye Xakalashe

Supervisor: Prof. Merete Tangstad

Co-supervisor: Dr. Jafar Safarian

Thesis for the degree of Master of Science

NORWEGIAN UNIVERSITY OF SCIENCE AND TECHNOLOGY

FACULTY OF NATURAL SCIENCES AND TECHNOLOGY

DEPARTMENT OF MATERIALS SCIENCE AND ENGINEERING

TRONDHEIM, SPRING 2011

Acceptance

The undersigned have examined the thesis entitled **"Removal of Phosphorus from Silicon Melts by Vacuum Refining"** presented by **Buhle Sinaye Xakalashe**, a candidate for the degree of Master of Science (Silicon and Ferroalloy Production) and hereby certify that it is worthy of acceptance.

Examiner 1

Date

Examiner 2

Date

Acknowledgements

I am humbled and simultaneously delighted to be in a position to express my sincere gratitude to the individuals and organisation(s) listed below for their support during my studies and particularly during the compilation of this thesis.

First and foremost I would like to thank my supervisors Professor Merete Tangstad and Doctor Jafar Safarian for the excellent guidance and support throughout this project. Moreover, I would like to extend a heartfelt gratitude to Prof. Merete Tangstad for including me in both the SimanTiAl team and Basic team. I would also like to thank the members of the groups for their invaluable input into my work.

I would also like to thank Torild Krogstad and Syverin Lierhagen for conducting the ICP-MS sample preparation and chemical analysis. Moreover, I extend my appreciation to Ciara Modanese and Professor Marisa di Sabatino for conducting the GDMS chemical analysis. Dr Erlend Nordstrand and Lars Jakobsson always showed interest in my work and offered support when needed and this is greatly appreciated.

Brit Wenche Meland is highly acknowledged for her support during my studies at the department of materials science and engineering, NTNU. Mange Takk!!

This work is a part of the BASIC project and I am very grateful for the funding for this work. Moreover, I am very grateful to Mintek for funding my master studies at NTNU.

I would like to thank my friends for being part of my life. In the fear of omitting any of you I express my gratitude to all of you who have had a positive impact in my life.

Last but not least I am thankful to my family for their love and support. I am also thankful for the values and principles instilled in me. I am particularly thankful to my mother and my late grandmother; words can't describe the magnitude of my appreciation, I dedicate this work to you. Ndiyabulela!!

SUMMARY

Induction vacuum refining testwork has been carried out for the removal of phosphorus from silicon melts. This work is of interest for the production of solar-grade silicon since phosphorus is hard to remove from silicon and is an important impurity in solar cells. The primary objective of the testwork was to study the effect of iron on phosphorus removal from silicon via induction vacuum refining.

The experiments were carried out through vacuum induction melting of high purity silicon with additions of phosphorus and iron to render blends with a phosphorus content of approximately 20 ppmw, and different iron contents as follows: 0 ppmw, 500 ppmw, 2000 ppmw and 5000 ppmw. The investigated temperatures and pressure were as follows, 1773 K - 1873 K and 0.5± 0.2 Pa, respectively. Holding times at the temperature of interest varied between 0 s and 7200 s. A total of 24 experiments were carried out. Each experiment had a batch mass of 0.3 kg. A graphite crucible with an inner diameter of 0.064 m was employed in the testwork. Three different analytical techniques were employed for chemical analysis of the experimental samples and these included Inductively Coupled Plasma Mass Spectroscopy (ICP-MS), Glow Discharge Mass Spectrometry (GDMS), and resistivity measurement.

ICP-MS seemed to be to be the most consistent of the analytical techniques employed for the chemical analysis of the samples. The experimental results showed that the starting phosphorus content subsequent to melting was approximately 15.5 ppmw. Moreover, the phosphorus content decreased to 1.5 ppmw after vacuum treatment at 1873 K and at a holding time of 7200 s. The removal of phosphorus was found to be substantial at 1873 K in comparison to that achieved at 1773 K. The removal of phosphorus from silicon via induction vacuum refining seems independent of iron concentration for iron concentrations of up to 5000 ppmw. The rate constants for phosphorus removal were determined to be 8.4×10^{-6}m/s and 2.5×10^{-6}m/s at 1873 K and 1773 K respectively. The removal rate of phosphorus was found to follow a first order equation where the monatomic gas species P is the predominant phosphorus species in the gas phase. It was proposed that the overall removal rate of phosphorus from silicon melts is controlled by free evaporation from the silicon melt surface.

Table of Contents

LIST OF FIGURES

LIST OF TABLES

LIST OF SYMBOLS AND ABBREVIATIONS

Symbol	Description
GDMS	Glow discharge mass spectrometry
ICP-MS	Inductively coupled plasma mass spectroscopy
ppmw	parts per million weight
A	Surface area of the gas-liquid interface
β_i	Separation coefficient of coefficient for component i
ε_i^j	Activity interaction coefficient
f_i	Henry activity coefficient of solute relative to 1% (Mass fraction) in an infinitely dilute solution
ΔG^o	Standard Gibbs free energy
K	Equilibrium constant
k_i	Total mass transfer coefficient of component i , (i = P, P_2, Si) [m/s]
γ_i	Activity coefficient for component i
N	Molar fraction
p	Pressure
P	Element or monatomic gas of phosphorus
p_i^*	Saturation vapour pressure for component i
p_i	Partial vapour pressure for component i
p_i^e	Equilibrium partial pressure of gas species $i\,(i = P, P_2, P_4)$

CHAPTER 1

INTRODUCTION

The unsustainable nature of fossil fuels as an energy source, from the point of view of future availability and environmental impact, has spurred an interest in diversification of energy sources, with particular interest in renewable energy. The photovoltaic (PV) industry is a player in the renewable energy segment, and the electricity generation from photovoltaics (solar cells) is deemed to be one of the key technologies of the 21st century [1]. Photovoltaic solar electricity presents an elegant means for electricity generation, as there are no moving parts, zero emissions, and no noise.

The photovoltaic industry is booming, growing at double-digit growth rates per annum [2], and is anticipated to maintain this boom for years to come [3], [4]. The dominant material used in PV cells is silicon, particularly multi-crystalline silicon [5]. The multi-crystalline silicon market share for PV cell production accounted for more than half of the total PV materials in 2010 [6]. Its preference over mono-crystalline silicon is due to lower production costs while maintaining relatively high energy conversion efficiency as a solar cell. The dominance of the crystalline silicon can be attributed to the maturity of the technology, and lower direct production costs, with a potential for further reduction in costs compared to other photovoltaic technologies [7]. Crystalline silicon is expected to maintain its lead in the near future [8], [9].

Until 1997, the silicon used in the production of solar cells was sourced from the waste stream of the electronic industry [1]. Subsequently, this became unsustainable due to a mismatch in supply-demand of silicon between the PV industry and the electronic industry, and the costs associated with production [1]. Moreover, the chemical purity requirements of electronic-grade silicon are much more stringent than those of solar-grade silicon. Consequently, technologies for a new silicon feedstock, the solar-grade silicon, tailored for the PV market had to be developed. Two main routes have been developed, or are currently under development, exclusively for the industrial production of silicon for the PV industry, and these are the chemical route and the metallurgical route [1]. An appraisal of these processing routes is given in this report.

The precursor material for both electronic-grade silicon and solar-grade silicon is metallurgical-grade silicon. Once solar-grade silicon is produced, the subsequent processing steps are as follows: wafer production, solar cells manufacture. Solar cells are assembled into solar modules for electricity generation. The flowsheets for the production of silicon solar cells from quartz via both the chemical route and the metallurgical route are shown in Figure 1.

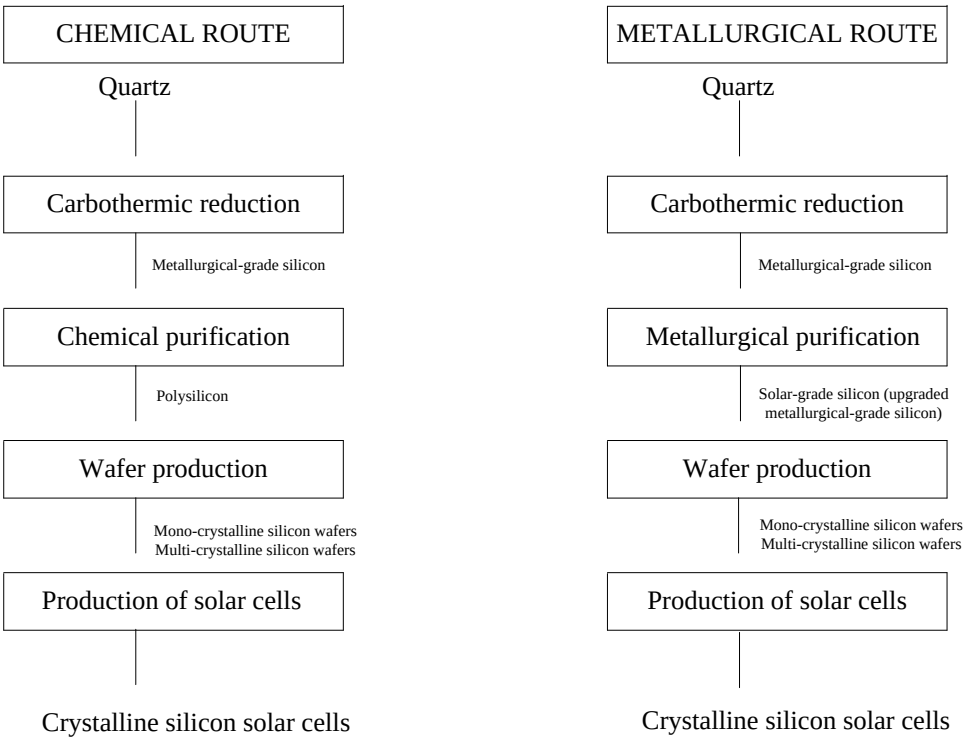

Figure 1: Stages for the production of crystalline silicon solar cells from quartz

1.1 Silicon and its applications

Silicon is the second most abundant element in the earth's crust, second only to oxygen. It is naturally found as fairly pure silicon dioxide and as silicates. The silicon dioxide is found as huge deposits of quartzite or quartz sand. Moreover, many rocks contain quartz crystals. Therefore, it can be concluded that the resources of silicon are virtually unlimited (although purity varies considerably).

The main applications of silicon are as follows: deoxidation and alloying of steel and cast iron, alloying of aluminium, raw material in the chemical industry, and raw material in the semiconductor industry (electronic devices and photovoltaic cells). A fair share of the silicon produced industrially is in the form of ferrosilicon, while the rest is as metallurgical-grade

silicon. Metallurgical-grade silicon is the precursor material for polycrystalline or solar-grade silicon used in the photovoltaic industry.

1.2 Industrial production of metallurgical-grade silicon

Silicon is produced industrially by carbothermic reduction of silicon dioxide in submerged-arc electric furnaces. Feed materials include a silicon source such as quartz, and a typical reductant blend comprising coke, coal, charcoal, and wood chips. Feed materials are impure, and impurities are carried to a certain extent to the silicon product stream.

A typical industrial silicon furnace has a shell diameter of about 10 m. Three pre-baked carbon electrodes, submerged into the charge materials, supply a three-phase current that heats the charge materials up to about 2 000^{o}C. At this temperature, silicon dioxide is reduced to molten silicon. The furnaces are operated such that there is a layer of solid material (outer reaction zone) on top of the molten bath (inner reaction zone) to maximize the silicon yield. The silicon is tapped from the furnace through a tap-hole at the bottom, and refined by slag treatment or gas purging. During refining, inclusions are removed, and the composition is adjusted to the specified value. Subsequent to refining, the molten alloy is allowed to cool in a mould, and then crushed to a specific size. Metallurgical-grade silicon has a typical specification of 98.5–99.5% for Si [10]. Typical impurities in metallurgical-grade silicon include carbon, alkali-earth and transition metals, as well as boron and phosphorus [11].

A by-product of the silicon smelting process is condensed silica fume. A silicon furnace produces about 0.2 to 0.4 tons of condensed silica fume per ton of silicon metal. The fume reports to the filter plant where it is collected. Condensed silica fume has found a wide array of applications in industry. Figure 2 shows a typical industrial silicon furnace.

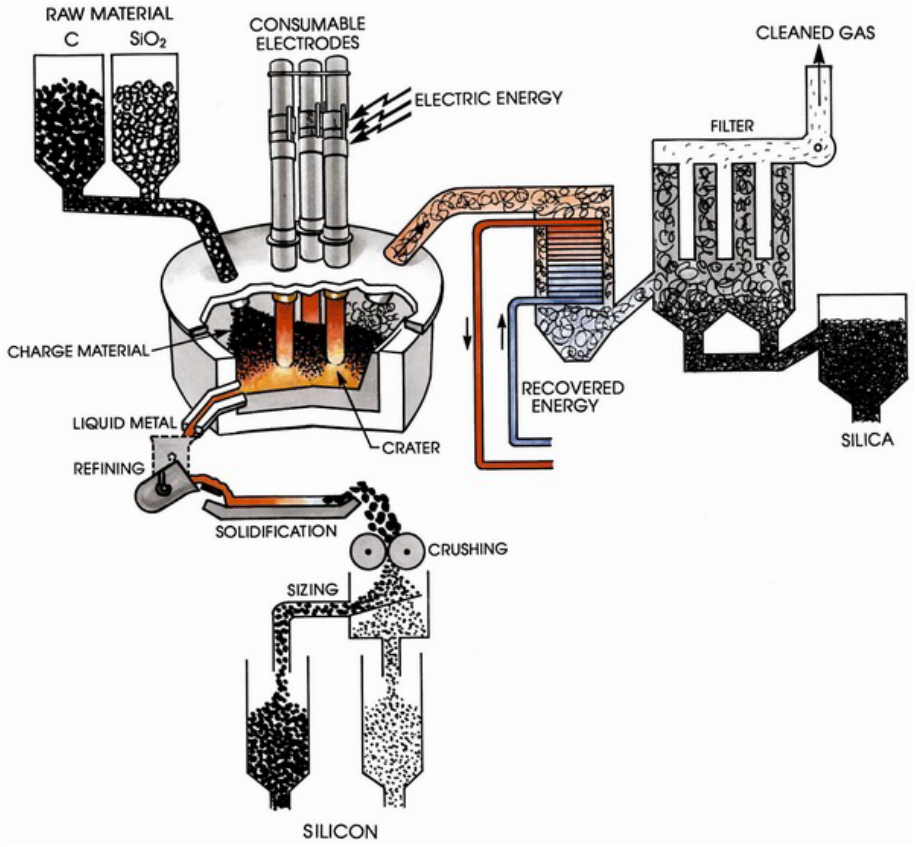

Figure 2: Typical plant layout: industrial production of metallurgical-grade silicon [12]

The electrical energy consumption for the production of metallurgical-grade silicon is 11–13 MWh/ton of silicon metal. The energy consumption per ton of alloy is reduced significantly with increasing iron content in the silicon alloy product. The off-gas from the silicon furnace has an energy content of the same order of magnitude as the electrical energy input to the furnace. The off-gas may be directed into an energy recovery system, and can be used to produce hot water or saturated steam for heating, or superheated steam for electricity generation.

Metallurgical-grade silicon is produced in excess of 1 million metric tons/year at a cost of few $/kg depending on quality, purity, and particle size. Metallurgical-grade silicon is produced in countries with cheap electricity, reductants, and good quartz deposits [10]. Demand for metallurgical-grade silicon is primarily from the aluminium and chemical industries, and a small fraction is refined into semiconductor-grade silicon [1]. However, this picture is expected to change in the future, as the fastest growing market for silicon metal is the

photovoltaic market, with projected consumption exceeding current silicon consumption for all other applications combined by 2020 [13].

1.3 Refining of metallurgical-grade silicon to solar-grade silicon

Impurities play a vital role in silicon solar cells. Impurities such as boron and phosphorus, in small amounts, are desirable for the formation of the p-n junction that is necessary for electricity generation in a silicon solar cell, while other impurities have adverse effects on solar cells. Impurities can lead to the formation of defects, and enhance the formation of dislocations, which act as recombination centres of photo-carriers and can compromise both mechanical and electrical properties as well as decrease the solar cell efficiency [6[14] Moreover, impurities in solar cells generally introduce allowed levels into the forbidden gap and thereby act as recombination centres, and an increased density of such centres decreases the cell efficiency [15]. The effect of metallic impurities on silicon solar cells is shown in Figure 3.

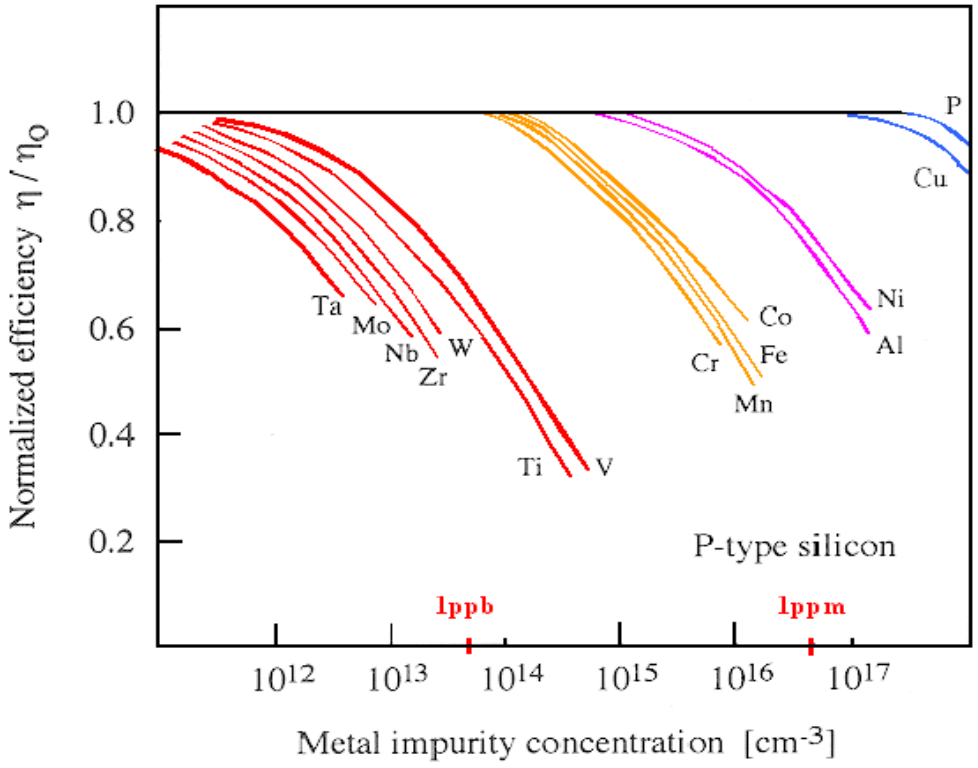

Figure 3: Silicon solar cell performance as a function of secondary impurities in p-type silicon[15]

The metal impurity concentration given in Figure 3 is expressed as the number of atoms of impurity per cm^3. Albeit some impurities can reduce the cell performance when present in extremely low concentrations, others can be tolerated at higher levels. The concentrations of these impurities are much lower compared to impurity concentration found in metallurgical-grade silicon (see Table 1). Therefore, refining of metallurgical-grade silicon is a necessary step [11]. However, these impurities are higher than the impurity levels in electronic-(semiconductor-) grade silicon, as shown in Figure 3. It is from this position that potential exists for the production of less expensive and less pure solar-grade silicon, tailored for the photovoltaic market. It must be noted that solar-grade silicon does not have formal specifications; acceptable concentrations of impurities are usually reported instead. The solar-grade silicon analyses reported in Table 1 provide a guideline rather than a specification for solar-grade silicon.

Table 1 Typical chemical analyses of silicon grades for the semiconductor industry

Element	Metallurgical-grade silicon[15] (ppm)	Solar-grade silicon[7[16] (ppm)	Polycrystalline solar-grade silicon[18]	Electronic-grade silicon[16] (ppm)
Si*	99	99.99 - 99.999 9	99.999 99	99.999 999 999
Fe	2 000–3 000	<0.3		<0.01
Al	1500–4 000	<0.1		<0.0008
Ca	500–600	<0.1		<0.003
B	40–80	<0.3		<0.0002
P	20–50	<0.1		<0.0008
C	600	<3		<0.5
O	3000	<10		
Ti	160–200	<0.01		<0.003
Cr	50–200	<0.1		

* Si content in mass %

The process for obtaining polycrystalline solar-grade silicon is divided into the chemical route and the metallurgical route, as mentioned previously. These processes will be discussed in detail in the following sections.

1.3.1 Chemical route

The traditional Siemens process is the baseline process for the production of polysilicon. The process was originally developed for the production of electronic-grade silicon in the 1950s.

The production scheme is as follows: gasification of metallurgical-grade silicon, distillation, and deposition of ultra-pure silicon. The detailed processing sequence is that fine metallurgical-grade silicon particles are fluidized with hydrochloric acid, in the presence of a catalyst, to produce trichlorosilane according to reaction (1.1).

$$Si + 3HCl = SiHCl_3 + H_2 \quad (1.1)$$

The trichlorosilane liquid undergoes multiple fractional distillation to produce a semiconductor-grade trichlorosilane. The semiconductor-grade trichlorosilane is then reduced by hydrogen in a Siemens reactor, and silicon is deposited in a fine-grained polycrystalline form on an electrically heated inverse U-shape silicon rod ($T > 1100^oC$) in a cooled Siemens reactor [15]. The deposition reaction is shown in reaction 2.

$$SiHCl_3 + H_2 = Si + 3HCl \quad (1.2)$$

The latter step is energy intensive, and has a low yield. The energy consumption of the Siemens process is in excess of 100 kWh/kg Si [1[12]. A typical Siemens process flowsheet, as described above, is shown in Figure 4.

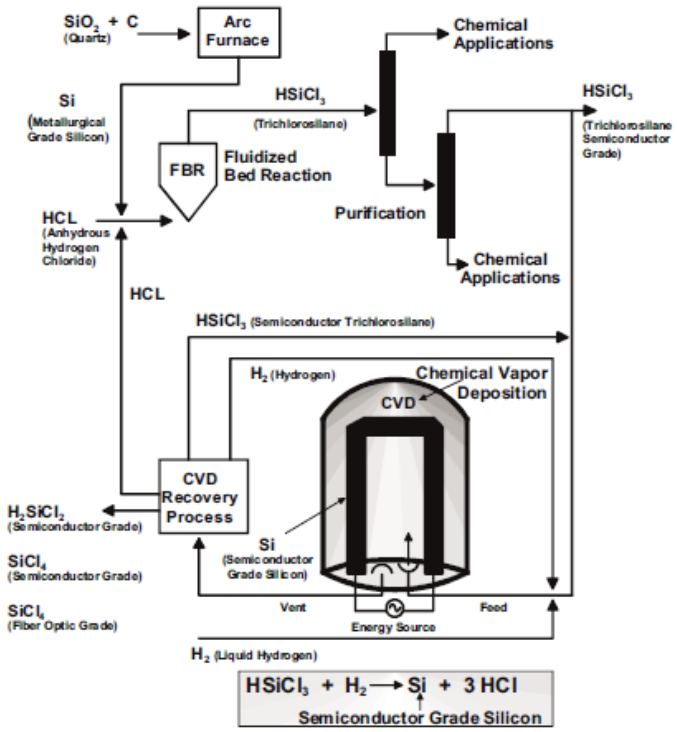

Figure 4: Typical flowsheet for industrial polysilicon production via the Siemens

process[10]

There have been advances in chemical-route technologies targeted at the production of solar-grade silicon. The highly volatile silane (SiH_4) can be used instead of the trichlorosilane during decomposition, and this has advantages over the use of trichlorosilane [10]. One process developed for the production of low-cost solar-grade silicon involves deposition in a fluid bed reactor instead of deposition in the Siemens reactor. The fluid bed reactor is more energy efficient; it produces more silicon per volume of reactor; it is a continuous process rather than a batch process; and, unlike the Siemens process, which requires the breaking of polysilicon rods, the grains produced in the fluidized bed reactor are in a usable form [17]. The processes mentioned in this section are amongst those that are currently used in industry; there are other emerging chemical processes that have been omitted [1[10]. The industrial processes discussed above, including the Siemens process, produce polysilicon with a purity of 99.999 99% for both the photovoltaic market and the electronic industry. Polysilicon under relaxed operation can be produced, but such a polycrystalline material would only be suitable for the solar industry. In 2006, the solar industry surpassed the semiconductor industry as the largest consumer of polysilicon [18]. The Siemens process accounted for about 78%, and the fluidized bed reactor for about 16% of polysilicon produced in 2008. The total polysilicon produced in 2008 was approximately 75 000 metric tons, of which 45 000 metric tons was used in the photovoltaic industry [19].

Other than the high energy consumption, the major problem with the chemical route is that it involves production of toxic and corrosive compounds; examples include chlorosilanes and hydrochloric acid [1]. The developments in the chemical route are at advanced stages compared to the metallurgical route that will be discussed in the following section.

1.3.2 Metallurgical route

The metallurgical route entails obtaining solar-grade silicon directly from metallurgical-grade silicon via a series of metallurgical refining steps. Solar-grade silicon produced via the metallurgical route is often referred to as upgraded metallurgical-grade silicon. The energy consumption of the metallurgical route is expected to be significantly lower than that of the Siemens process [1].

Most metallic elements have a low segregation coefficient in silicon, which means that the solid rejects impurities into the liquid during crystallization. The refining techniques based on this principle include both directional solidification and acid leaching. Directional solidification can also be used as a casting step for preparation of single-crystal and multi-crystal ingots from which wafers are prepared.

Other impurities have high segregation coefficients in silicon; these include boron, carbon, oxygen, and phosphorus. Therefore, such impurities cannot be removed from silicon via the above-mentioned refining techniques. Phosphorus can be volatilized from silicon, and removed via vacuum refining. Boron can be removed from silicon by slag refining, or via plasma refining where carbon and oxygen are also removed. It is common in the metallurgical route to employ high-purity raw materials, *i.e.* purified quartz, carbon black, and high-purity electrodes; this renders low impurity levels in the upgraded metallurgical-grade silicon product.

Since the refining techniques used in the metallurgical route tend to be effective in removing specific impurities, combinations of the refining steps are employed in industry for effective refining of metallurgical-grade silicon to solar-grade silicon. The metallurgical route has the potential to become dominant in the production of solar-grade silicon. Polycrystalline solar-grade silicon sourced from the metallurgical route accounted for less than about 8% of the total production in 2008 [19].

1.4 Scope of thesis

As mentioned previously, phosphorus has a high segregation coefficient, 0.35, and can therefore not be effectively removed from metallurgical-grade silicon by directional solidification. Moreover, phosphorus is an important dopant for silicon solar cells; therefore, control on the phosphorus content is essential in solar-grade silicon. Due to high vapour pressure of phosphorus, vacuum refining is an alternative method for the removal of phosphorus from metallurgical-grade silicon. The application of vacuum refining to phosphorus removal from silicon method is not well established in industry, and has potential for further development.

In ferrosilicon smelting, a majority of phosphorus reports to the metal stream due to the formation of iron phosphorus compound. As established previously, iron is the major impurity

in metallurgical-grade silicon; however, the concentrations are much lower than those found in ferrosilicon. The question remains as to whether iron has an effect on the removal of phosphorus from metallurgical-grade silicon.

This master thesis project focuses on vacuum refining of silicon melts prepared from blends of high purity silicon with additions of phosphorus and iron, such that the concentrations of iron and silicon are in the range of these elements in metallurgical-grade silicon. The primary objective of this project was to study the effect of iron on the removal of phosphorus from silicon via vacuum refining in the absence of other impurities. The work entailed the following:

- Investigation of the effect of temperature, pressure, time, and iron concentration on the removal of phosphorus from silicon melts.
- Determine the phosphorus vacuum refining kinetic parameters.
- Characterise the analytical techniques for chemical analysis of the elements of interest in the phosphorus removal from silicon

A matrix showing a combination of parameters that were investigated is given in the table below, the phosphorus content of the silicon melts was kept at 20 ppm.

Table 2 Investigated parameters

Temperature (K)	Pressure (Pa)	Fe concentration(ppm)	Time (s)
1773, 1873	0.5	0, 500, 2000, 5000	0, 1800, 3600, 7200

CHAPTER 2

LITERATURE OVERVIEW

An overview of previously published work in phosphorus removal from silicon is given in this chapter. Moreover, the theoretical principles relevant to this thesis are presented. Both the theory and literature presented in this chapter are essential for the discussion and interpretation of the results.

2.1 Literature survey

Vacuum refining is a viable alternative process for the removal of phosphorus from silicon melts. The removal of phosphorus from silicon melts by vacuum treatment has been investigated through experimental work employing different melting techniques which include electron beam melting and induction melting. The silicon melts investigated are predominantly metallurgical-grade silicon, and a few silicon-phosphorus systems. According to the author, refining of silicon-phosphorus melts with iron addition has never been reported in literature.

2.1.1 Removal of phosphorus from silicon melts by vacuum refining through induction melting

Suzuki et al. [20] undertook metallurgical-grade silicon vacuum refining at temperatures of 1450^{o}C and 1550^{o}C under vacuum pressure of 0.027Pa over various refining times. Considerable removal of P, Ca and Al was achieved. A phosphorus reduction from 32 ppmw to 6-7 ppmw over a holding period of 6 hours was observed. The effect of change in temperature was minimal on P removal rate. However, the removal rate of both Ca and Al showed an increase with increasing temperature. Moreover, rate constants were calculated for P, Ca and Al evaporation (assuming first order reaction for the evaporation of the elements under investigation). It was also suggested that the overall evaporation rate of P and Ca is controlled by the diffusion of these elements through liquid silicon to the liquid-gas interface.

Yuge et al. carried out metallurgical-grade silicon refining under vacuum investigating the removal of P, Ca and Al at a pressure of 0.014-0.016 Pa and at temperatures of 1500^{o}C, 1550^{o}C and 1642^{o}C [21]. Both P and Ca could be removed to less than 0.1 ppmw at 1642^{o}C over a period of 7 hours. It was found that change in temperature had a higher effect on the removal rate of Al and Ca than P. The authors also carried out the silicon refining experiments at the following conditions: 4 and 190 Pa at temperatures of 1460^{o}C and 1550^{o}C. Phosphorus removal was found to be significantly slow and removal to below 1ppmw was achieved over a period of 17 hours. The rate constants for the removal of P, Al and Ca were calculated on the basis that the removal of the elements followed a first order equation. Moreover, they estimated the activation energies for the removal of the elements as follows: 130kJ/mol for phosphorus, 147kJ/mol for calcium and 186kJ/mol for aluminium. The authors also showed that the overall rate of removal of the elements of interest is controlled by the diffusion in molten silicon and evaporation from the silicon surface.

Luyima [22] carried out metallurgical-grade silicon refining experiments to study the removal of phosphorus. The operating conditions of interest were a pressure of 20 Pa and temperatures of 1773 K and 1873 K. A phosphorus reduction from 15 ppmw to 3 ppmw after 3.5 hours at 1873K was achieved. The removal rate constant for phosphorus removal from molten silicon was determined, and expressed by a first order equation. The activation energy for phosphorus removal was estimated to be 264 kJ/mol. Moreover, it was suggested that the overall removal rate of phosphorus is controlled by free evaporation from the silicon melt surface.

Safarian and Tangstad [23] performed experimental work to study vacuum behaviour of the dissolved elements in molten silicon. Metallurgical-grade silicon was used in the testwork. The temperature and pressure investigated was 1500^{o}C and 2-4 Pa respectively. It was observed that the concentrations of B, Fe, Ti, Al and Cu were not significantly reduced within 2 hours of refining. Whereas, Ca, Mg, Na, Mn, Zn, Pb, Sn, Bi, Sb, As, K and P were evaporated with different rates and different amounts. Phosphorus removal under the experimental conditions was reduced from 33ppmw to 16ppmw over a period of 2 hours. Moreover, the rate constant for phosphorus removal was determined to be 6.3 x10^{-5} m/s. The authors reported that the evaporation of volatile elements from the molten silicon takes place in two stages: a fast initial stage followed by a slower stage. Lastly, the authors proposed that free evaporation of elements at the melt-gas interface controls the removal rate of elements in

the first stage, while mass transfer of elements in the melt or a combination of mass transfer and the evaporation of elements is rate limiting.

Zheng et al. investigated the elimination of phosphorus by vaporizing from silicon. The melt investigated was a Si-P alloy made from electronic grade silicon. The experimental parameters were as follows: temperature of 1873 K, holding time of 1 hour and pressure ranges of 600-800 Pa, 60-80 Pa, 6-8 Pa and 0.6-0.8Pa. The experimental results showed that phosphorus mass fraction can be decrease from 460 ppmw to 10 ppmw at a pressure of 0.6-0.8 Pa. It was established that at high phosphorus concentration, the phosphorus removal is quite dependent on high chamber pressure while it is independent on low chamber pressure since phosphorus evaporates from molten silicon as a gas species P_2 at a relatively high phosphorus concentration, and as a gas species P at low phosphorus content.

2.1.2 Removal of phosphorus from silicon melts by vacuum refining through electron beam melting

Ikeda and Maeda [25] studied the purification of metallurgical-grade silicon using electron beam melting at a pressure of 0.01 Pa for 30 minutes. The removal of impurities was as follows: 75% for aluminium, 90% for carbon, 89% for calcium and 93% for phosphorus. Phosphorus was reduced to 3 ppmw. The removal rate was expressed as a first order equation for the removal of carbon, calcium and aluminium, while a second order equation was employed for phosphorus removal.

Hanazawa et al. [26] investigated phosphorus evaporation from molten metallurgical-grade silicon by electron beam irradiation under a pressure of 0.001-0.01 Pa. The electron beam irradiation made it possible for secure a higher temperature of free liquid surface, which rendered an efficient removal of phosphorus. The authors demonstrated a removal of phosphorus from 25 ppmw to less than 0.1 ppmw within 3.5 hours. Phosphorus removal rate was found to increase with an increase in electron beam power density and was found to be first order with respect to phosphorus concentration. Moreover, it was suggested that the removal rate of phosphorus was controlled by free evaporation from the surface of molten silicon.

Pires et al. [27] utilised electron beam melting to refine metallurgical-grade silicon under high vacuum pressure ranging between 0.0001 Pa and 0.01 Pa. They demonstrated removal of all the impurities with more than 95% with the exception of boron. Phosphorus removal from 38 ppmw to 0.39 ppmw was achieved.

Miyake et al. [28] investigated the removal of phosphorus and antimony from silicon by electron beam melting at a pressure of 5-7 Pa. They reported removal of phosphorus from 200 ppmw to about 1 ppmw and antimony removal from 300 ppmw to below 0.1 ppmw within an hour. They observed similar removal rates under high vacuum operation of 0.001 Pa.

2.2 Thermodynamics of phosphorus removal from silicon

Vacuum refining is an established process in metallurgy for the purification of molten metals. Examples of application of vacuum refining include deoxidation and degassing of liquid steel [29], and removal of arsenic and antimony from liquid copper [30]. The difference in the vapour pressure of the liquid metal components at high temperatures is the basic principle of crude metal vacuum distillation [23]. The relationship between saturation vapour pressure and temperature for a sample of pure elements is shown in Figure 5.

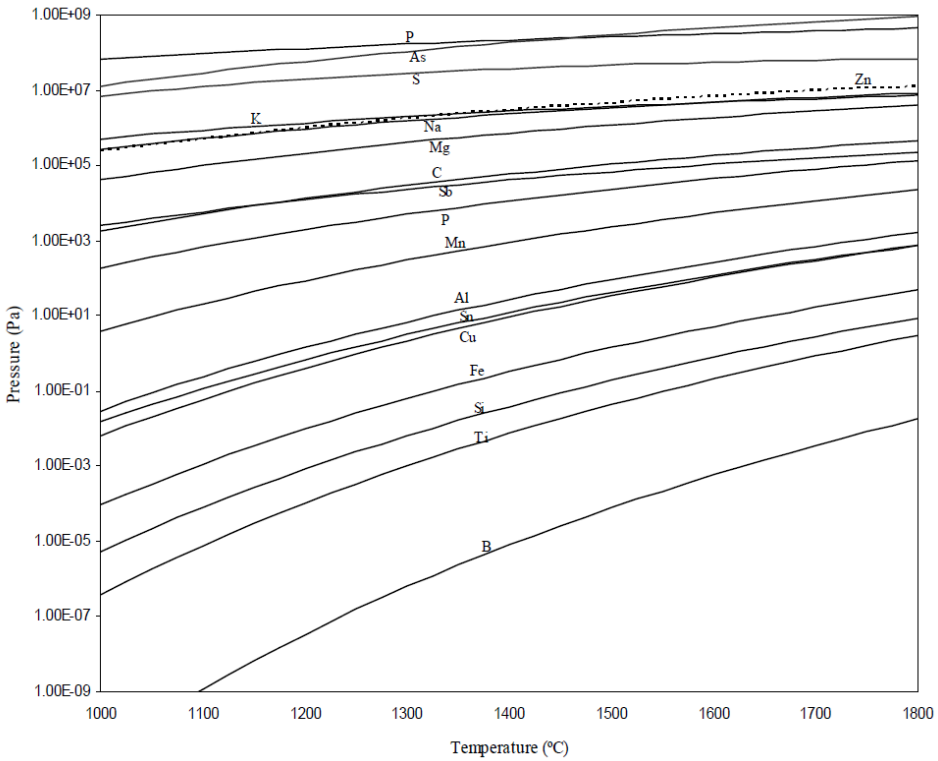

Figure 5: Theoretical relationship between saturation vapour pressure and temperature for pure elements [23]

The curves in the figure have been calculated using reported thermodynamic data on saturation vapour pressures of pure substances [31]. As can be seen from the figure the saturation vapour pressure of many elements is higher than that of silicon over the temperature range of choice. Therefore, removal of many elements from liquid silicon seems possible. It must be noted that it is possible to remove elements with lower vapour pressure than silicon such as boron; to achieve the removal of such elements it is necessary to convert the elements into volatile compounds [29]. Of particular interest for this thesis is the saturation vapour pressure of phosphorus relative to that of silicon. At the same temperature, the saturation vapour pressure of phosphorus is much higher than that of silicon. At 1732 K, silicon begins to melt and phosphorus sublimes. In theory, phosphorus separation from silicon via vacuum distillation seems possible.

2.2.1 Possibility of Si-P alloy separation

Wei et al. [32] appraised the possibility of separating phosphorus from silicon melt by considering a binary alloy, consisting components A and B. Due to interaction between the two elements, the actual (partial) vapour pressure of A and B are not equal to their saturation vapour pressure. To establish the partial vapour pressures of A and B, the activity a and the molar concentration N of A and B in A-B binary alloy must be considered. The partial vapour pressures of A and B in A-B binary alloy are as follows:

$$p_A = p_A^* a_A = p_A^* N_A \gamma_A \tag{2.1}$$

$$p_B = p_B^* a_B = p_B^* N_B \gamma_B \tag{2.2}$$

Where p_A and p_B are the partial vapour pressures of A and B, a_A and a_B are the activities of A and B, p_A^* and p_B^* are the saturation vapour pressures of A and B, N_A and N_B are the molar fraction of A and B, and γ_A and γ_B are the activity coefficients for A and B, respectively.

From equations (2.1) and (2.2), the following equation can be deduced:

$$\frac{p_A}{p_B} = \frac{p_A^* N_A \gamma_A}{p_B^* N_B \gamma_B} \tag{2.3}$$

Assuming the following,

$$\beta_A = \frac{p_A^* \gamma_A}{p_B^* \gamma_B} \tag{2.4}$$

Then

$$\frac{p_A}{p_B} = \beta_A \frac{N_A}{N_B} \tag{2.5}$$

β_A is a function of the ratio of the concentrations of elements in the two phases, which is related to the activity coefficients and vapour pressures of the elements. Moreover, β_A is defined as the separation coefficient of A, which can be used to determine whether element A can be removed from A-B binary alloy by vacuum distillation.

- When $\beta_A = 1$, the composition of A and B in vapour and liquid phase are the same. Element A cannot be separated from element B.
- When $\beta_A > 1$, the composition of A in the vapour phase is more than in liquid phase, element A can be separated from element B. Element A is concentrated in the vapour phase, and element B is concentrated in the liquid phase. The bigger the value of β_A is, the higher the removal efficiency will be.
- When $\beta_A < 1$, the composition of A in the liquid phase is more than in the vapour phase, element A can be separated from element B. Element A is concentrated in the liquid phase, and element B is concentrated in the vapour phase. The smaller the value of β_A is, the higher the removal efficiency will be.

For P-Si binary alloy, $\beta_A > 1$, the content of phosphorus in the vapour phase is more than in the liquid phase, phosphorus can be separated from silicon. Phosphorus is concentrated in the vapour phase, and silicon is concentrated in the liquid phase. Wei et al. [32] calculated the separation coefficient of phosphorus in silicon phosphorus alloy for the temperature range 1373 to 2173 K and found $\beta_P >> 1$. It can be concluded that phosphorus can be completely separated from silicon by vacuum distillation.

2.2.2 Thermodynamics of phosphorus species from silicon melts

Miki et al. [33] investigated the thermodynamics of phosphorus in molten silicon and found that the Gibbs energy change of phosphorus dissolution into molten silicon is determined in the temperature range from 1723 to 1848 K by equilibrating a molten silicon-phosphorus alloy in a controlled phosphorus partial pressure and is expressed as follows:

$$\underline{\mathrm{P}}\ (\text{mass \%, in Si}) = \frac{1}{2}\mathrm{P_2\,(g)} \tag{2.6}$$

$$\Delta G_1^o = 139000(\pm 2000) - 43.4(\pm 10.1)T \tag{2.7}$$

Zheng et al. [24] discussed the evaporation of phosphorus from molten silicon and used equations (2.6) and (2.7) as a starting point. The Gibbs energy change has a relationship with reaction equilibrium for equation (2.6) as follows:

$$\Delta G_1^o = -RT\ln K = -RT\ln[(p_{P_2}^e / p_{atm})^{1/2} / f_P\,.mass\%] \tag{2.8}$$

The equilibrium partial pressure of species P_2 can be derived from equation (2.8):

$$p_{P_2}^e = p_{atm}\{f_P.mass\%.\exp[\frac{\Delta G_1^o}{RT}]\}^{-2} \tag{2.9}$$

The Gibbs energy change of the reaction from gas species P_2 to species P is as follows:

$$\frac{1}{2}\mathrm{P_2\,(g)} = \mathrm{P\,(g)} \tag{2.10}$$

$$\Delta G_2^o = 248000 - 59.4T \tag{2.11}$$

Similarly, the equilibrium partial pressure of species P can also be derived as follows:

$$\underline{\mathrm{P}}\ (\text{mass \%, in Si}) = \mathrm{P\,(g)} \tag{2.12}$$

$$\Delta G_3^o = 387000(\pm 2000) - 103(\pm 10)T \tag{2.13}$$

$$\Delta G_3^o = -RT\ln K = -RT\ln[(p_P^e / p_{atm}) / f_P\,.mass\%] \tag{2.14}$$

$$p_P^e = p_{atm}.f_P.mass\%.\exp[-\Delta G_3^o / (RT)] \tag{2.15}$$

The Gibbs energy change of the reaction from gas species P_2 to species P_4 is as follows:

$$2P_2\,(g) = P_4\,(g) \tag{2.16}$$

$$\Delta G_4^o = -229500 + 154.5T - 0.00313T^2 \tag{2.17}$$

Consequently, the equilibrium partial pressure of species P_4 can be analogised as follows:

$$\underline{P}\ (\text{mass \%, in Si}) = \frac{1}{4}P_4\,(g) \tag{2.18}$$

$$\Delta G_5^o = 81625 - 4.8T - 0.0008T^2 \tag{2.19}$$

$$\Delta G_5^o = -RT\ln K = -RT\ln[(p_{P_4}^e / p_{atm})^{1/4} / f_P\,.mass\%] \tag{2.20}$$

$$p_{P_4}^e = \{p_{atm}.f_P.mass\%.\exp[-\Delta G_5^o/(RT)]\}^4 \tag{2.21}$$

Where K is the equilibrium constant; p_{atm} is the atmospheric pressure (101325Pa), and f_P is the activity coefficient of phosphorus relative to 1% (mass fraction) in molten silicon. According to the Wagner Model:

$$\ln f_i = \sum_{j=2}^{n} \ln f_i^{\,j} = \sum_{j=2}^{n} \varepsilon_i^j x_j \tag{2.22}$$

Where ε_i^j is the activity interaction coefficient. When taking no account of the effect of other impurities, we have:

$$\ln f_P = \frac{\varepsilon_{P\ in\ Si}^P M_{Si}}{100 M_P} mass\% \tag{2.23}$$

Where:

$$\varepsilon_{P\ in\ Si}^P = 13.8(\pm 3.2) \tag{2.24}$$

The equilibrium partial pressures of species P, P_2 and P_4 can be calculated and plotted as a function of phosphorus concentration in Figure 6.

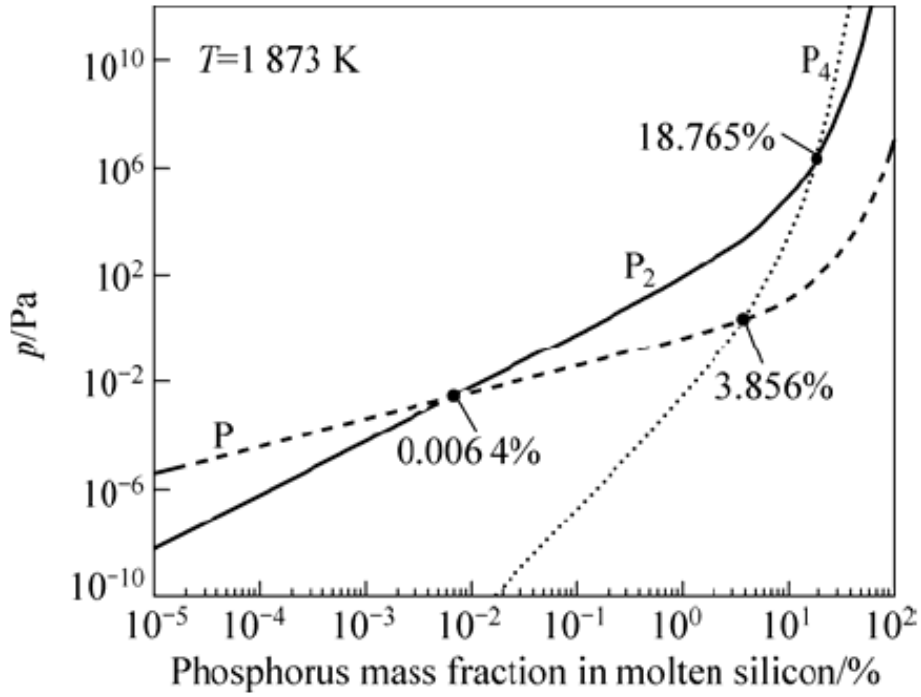

Figure 6: Equilibrium partial pressure of species P, P_2 and P_4 as a function of phosphorus concentration in molten silicon at 1873 K [24]

As shown in the figure above, monatomic gas species P will be dominant in the gas phase when the phosphorus concentration in silicon is less than 64 ppmw which is in agreement with the work done by Miki et al. [33] that for low phosphorus concentrations below 50 ppmw, monatomic phosphorus vapour dominates the gas phase at 1823 K. Species P_2 dominates the gas phase at phosphorus concentrations of 0.0064% - 18.765%. The partial pressure of species P_4 will be greater than that of species P when the phosphorus concentration is greater than 3.865%. Moreover, phosphorus species P_4 dominates the gas phase for phosphorus concentrations greater than 18.765%. Based on this discussion, the phosphorus gas species evaporating from molten silicon during processing of metallurgical-grade silicon are expected to be P and P_2 due to the concentration of phosphorus in metallurgical-grade silicon.

2.3 Kinetics of phosphorus removal from silicon

Thermodynamics alone does not suffice in evaluating the production efficiency of a process [23]. This is because thermodynamically feasible processes may be too slow to proceed practically.

As established from the thermodynamics of phosphorus in molten silicon for solar applications; the gas species of phosphorus evaporating from molten silicon are P and P_2, and follow first and second order kinetics, respectively [34]:

$$\frac{d[mass\%P]_1}{dt} = -\frac{A}{V}k_p[mass\%P] \tag{2.25}$$

$$\frac{d[mass\%P]_2}{dt} = -\frac{A}{V}k_{p_2}[mass\%P]^2 \tag{2.26}$$

Then,

$$\frac{d[mass\%P]}{dt} = -\frac{A}{V}(k_P[mass\%P] + k_{P_2}[mass\%]^2) \tag{2.27}$$

Where A is the surface area at the gas-liquid interphase, V is the volume of the silicon melt, k_p and k_{p_2} are the total mass transfer coefficients for gas species P and P_2, respectively. Rearranging and integrating equation (2.28) yields:

$$[mass\%P] = \frac{k_P}{-k_{P_2} + (k_{P_2} + k_P/[mass\%P]_o).\exp((A/V)k_P(t - t_o))} \tag{2.28}$$

The fundamental criterion is that the ratio of solute evaporation rate to solvent evaporation rate must exceed the ratio of their respective concentrations, N_i and N_{Si}, in the bulk liquid metal:

$$\frac{\nu_i}{\nu_{Si}} > \frac{N_i}{N_{Si}} \tag{2.29}$$

Where ν_i is the solute evaporation rate in kg/m^2.s and ν_{Si} is the solvent evaporation rate in kg/m^2.s.

The evaporation rate of an element is affected mainly by temperature and pressure [35]. Ma et al. [35] studied the kinetics on vacuum refining process of metallurgical-grade silicon using maximum evaporation rate, critical pressure and mean free path of phosphorus in the metallurgical-grade silicon at different temperatures. The main findings are reviewed in the section below.

2.3.1 Maximum evaporation rate of phosphorus in silicon melts

2.3.1.1 Relationship between maximum evaporation rate and temperature

When the total chamber pressure p is less than the saturation vapour pressure of a pure element p_i^* and the mean free path λ of the vaporised molecule is greater than the effective dimension l which is the distance between evaporating and condensing surface of the unit, the evaporation rate of the distilled element is maximum, and can be described by the following equation:

$$\nu_i = \alpha p_i^* [M_i / 2\pi RT]^{1/2} \tag{2.30}$$

Where ν_i is the evaporation rate in kg/m^2.s, M_i is the relative molecular mass of the distilled element, α is the evaporation coefficient, p_i^* is the saturation vapour pressure of the distilled element, R is the gas constant and T is the melt surface temperature. The evaporation coefficient ($0 < \alpha \leq 1$) is close to unity for a vapour with high molecular mass under vacuum conditions [24]. When the vapour evaporates into a finite pressure gas instead of evaporating into a vacuum, the evaporation coefficient will no longer be unity. Equation (2.30) is the Hertz-Langmuir-Knudsen equation, and holds under a special case of perfect vacuum for the evaporation of monatomic phosphorus gas species P from the free silicon melt surface [34]. Under these conditions all molecules evaporating are subsequently removed or condensed, and $\nu_i = \nu_{i,\max}$ where $\nu_{i,\max}$ is the maximum evaporation rate. Supposing that the evaporation coefficient α is 1, the maximum evaporation rate of each element contained in the investigated silicon melt is calculated in the temperature range of 1073 – 2173 K and presented in Table 3.

Table 3 Maximum evaporation rates of pure silicon and pure phosphorus at different temperatures

Temperature (K)	$\nu_{max,Si}$ (kg/m^2.s)	$\nu_{max,P}$ (kg/m^2.s)
1073	3.66E-12	1.92E+04
1173	1.52E-10	3.03E+04
1273	3.51E-09	4.43E+04
1373	5.08E-08	6.12E+04
1473	5.09E-07	8.07E+04
1573	3.79E-06	1.03E+05
1673	2.21E-05	1.26E+05
1773	1.05E-04	1.52E+05
1873	4.22E-04	1.79E+05
1973	1.47E-03	2.07E+05
2073	4.52E-03	2.35E+05
2173	1.25E-02	2.64E+05

As can be seen from the table above, the evaporation temperature has a significant effect on the maximum evaporation rate. The evaporation rate can be enhanced by several orders of magnitude with the temperature increment of 100 K. It can be concluded that phosphorus is volatilised quickly and concentrated into vapour phase. It appears relatively easy to separate impurity phosphorus from the silicon melt completely because the value of $\nu_{max,P}$ is 10^9 times greater than that of $\nu_{max,Si}$ in the investigated temperature range. It must be noted that during the evaporation of phosphorus from molten silicon, silicon will vapourise as well; this can be confirmed by the $\nu_{max,Si}$ values which also shows an increase with an increase in temperature (see Table 3). The kinetics of the vapourisation of silicon will not be treated in this literature overview for two main reasons firstly the evaporation of silicon is minimal, and secondly the focus of the thesis is on phosphorus removal.

2.3.1.2 Relationship between evaporation rate and pressure

The evaporation of metals or alloys can be enhanced by vacuum conditions [35]. Literature [24, [34,[35] has shown that the evaporation rate increases with a decrease of chamber pressure as shown qualitatively in Figure 7. When the pressure decreases to a specific value or below, the evaporation rate does not increase any more or increase at a negligible amount. This value is called the critical pressure p_{crit}, which is invaluable for the selection of

optimised pressure. The critical pressure means that $\nu_i = \nu_{i,\max}$ in practice. It increases with increasing temperature.

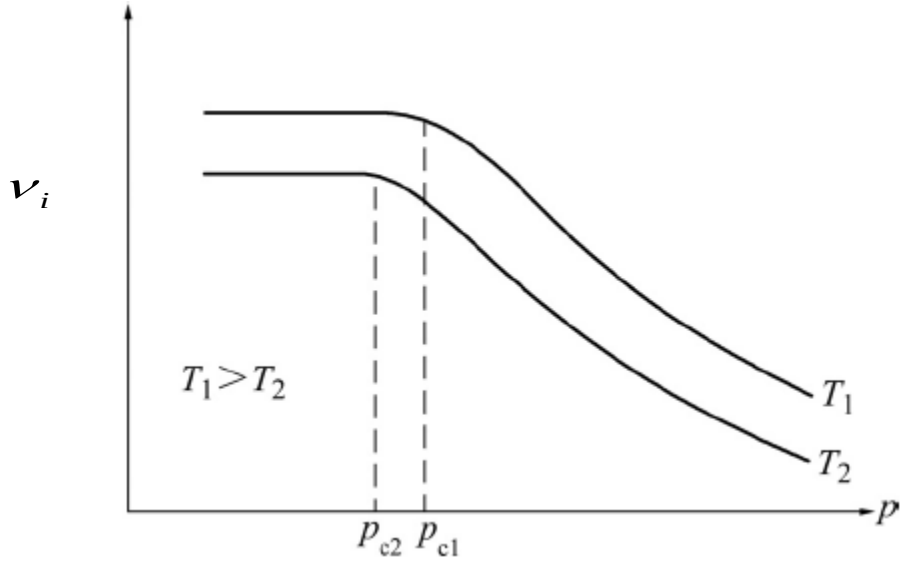

Figure 7: Relationship between evaporation rate and chamber pressure [35]

Moreover, the authors determined the critical pressure as follows:

$$p_{crit} = \frac{\kappa T}{\lambda \sigma \sqrt{1 + (M_m / M_g)}} \tag{2.31}$$

$$\sigma = \frac{\pi}{4}\left(\frac{d_m + d_g}{2}\right)^2 \tag{2.32}$$

Where M_m is the relative molecular mass of the metal vapour, M_g is the relative molecular mass of the residual gas vapour, d_m is the molecular diameter of the metal vapour, d_g is the molecular diameter of the residual gas vapour, σ is the molecular mean cross-section of the vapour, κ is the Boltzmann constant and λ is the mean free path. Argon was used as the protective gas when experiments were carried out, and the distance between evaporating and condensing surface was assumed to be 0.15 m in a vacuum refining of metallurgical-grade silicon. Argon was considered as the residual gas and λ was assumed to be 0.15 m. The critical pressures of the phosphorus in metallurgical-grade silicon were subsequently calculated employing equations (2.31) and (2.32) and are listed in Table 4.

Table 4 Relationship between critical pressure of pure metal and temperature [35]

Temperature (K)	$p_{crit,Si}$ (Pa)	$p_{crit,P}$ (Pa)
1073	1.761	2.121
1173	1.925	2.319
1273	2.089	2.516
1373	2.253	2.714
1473	2.417	2.912
1573	2.581	3.109
1673	2.745	3.307
1773	2.909	3.505
1873	3.073	3.702
1973	3.237	3.900
2073	3.401	4.098
2173	3.566	4.295

It can be seen from Table 4 that the critical pressure is directly proportional to temperature. The minimum chamber pressure should be less than 2.1 Pa to ensure the maximum evaporation rate of phosphorus reaches the range of 1.92×10^4-2.64×10^5 kg/m^2.s, while silicon volatilises at lower rates much smaller that the phosphorus evaporation rate [35].

2.3.2 Other factors that affect the removal rate of phosphorus in silicon melts

Since the most important factors regarding the removal rate of phosphorus removal from silicon have been discussed, namely temperature and pressure; other factors will be briefly appraised. During the refining of phosphorus from metallurgical-grade silicon, there are other impurities present such as Al, Ca, B and Fe which could affect the diffusivity and the activity of phosphorus in silicon. The major impurities in metallurgical-grade silicon such as aluminium, and calcium usually vapourise to some extent during vacuum refining for phosphorus removal [23, [25], iron is the exception as no vapourisation of iron takes place.

Zheng et al. [34] discussed factors affecting phosphorus removal from silicon, and listed them as follows in decreasing order: temperature, chamber pressure, geometry of silicon melt, holding time, and the original phosphorus concentration. The main findings are presented below.

The effect of geometry on phosphorus removal is usually expressed in terms of a ration A/V, where A and V are the surface area at the gas-liquid interphase and volume of the melt

respectively. The authors assumed a cylindrical crucible with diameter and height for the study. Phosphorus removal was found to increase with an increase in diameter to height ratio i.e. A/V ratio, silicon vapourisation is pronounced when diameter to height ratio exceeds 10.

Phosphorus removal is almost independent of the original concentration at temperatures above 2103 K. High initial phosphorus concentration renders a high removal rate of phosphorus, since phosphorus evaporates as species P_2 at high phosphorus concentration and as species P at low phosphorus concentration.

Zheng et al. [34] appraised the removal of phosphorus from silicon as summarised above on the basis of a model. The model as well as the mass transfer will be summarised in the following section.

2.3.3 Induction vacuum refining model and mass transfer

The model developed by Zheng et al. [34] for phosphorus evaporation from silicon melt by induction vacuum refining is shown in Figure 8, and details the transfer path of phosphorus during silicon refining.

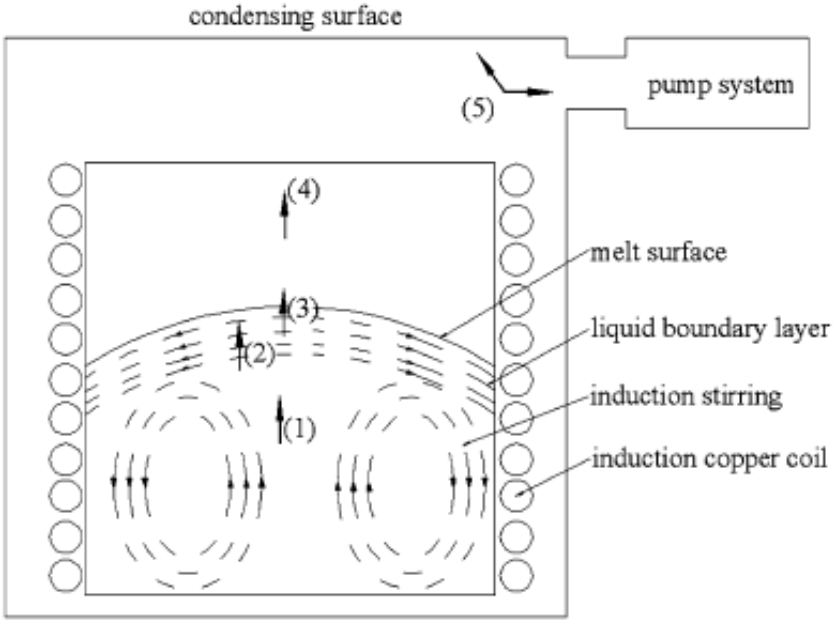

Figure 8: Illustration of the model detailing mass transfer steps of the phosphorus during the evaporation process [34]

As can be seen from the figure above, the transfer path of phosphorus during silicon refining entails five steps as follows:

(1) Transport of an atom through the melt to the neighbourhood of the metal surface.
(2) Transport across a liquid boundary layer to the melt surface.
(3) Vapourization from the free melt surface into the gas phase above the surface.
(4) Transport across a gas phase in the chamber.
(5) Condensation on the chamber inner surface or gas removal pump.

Silicon melt is in a rapid movement caused by induction stirring, therefore, step (1) is not rate limiting for evaporation of gas species P or P_2. Step (5) is also assumed not to be rate limiting due to condensation occurring on a very large area of cold surface and volatile components being pumped out. Consequently, steps 2 to 4 are considered to be rate limiting steps for phosphorus removal from silicon. The authors [34] evaluate each of these steps comprehensively. Of interest is the overall outcome of the evaluation. The total mass transfer coefficients of phosphorus species P and P_2 are as follows:

$$\frac{1}{k_P} = \frac{1}{k_{P,(2)}} + \frac{1}{k_{P,(3)}} + \frac{1}{k'_{P,(4)}} \tag{2.33}$$

$$\frac{1}{k_{P_2}} = \frac{1}{k_{P_2,(2)}} + \frac{1}{k_{P_2,(3)}} + \frac{1}{k'_{P_2,(4)}} \tag{2.34}$$

Where k_P is the total mass transfer coefficient of phosphorus gas species P, $k_{P,(2)}$ is the mass transfer coefficient of phosphorus gas species P in step (2), $k_{P,(3)}$ is the mass transfer coefficient of phosphorus gas species P in step (3) and $k'_{P,(4)}$ is the mass transfer coefficient of phosphorus gas species P relative to step (4). Similarly, k_{P_2} is the total mass transfer coefficient of phosphorus gas species P_2 and has its accompanying mass transfer coefficients for each step. The mass transfer coefficients for each step are as follows:

$$k_{P,(2)} = \sqrt{8D_{P(l)}v/\pi.r} \tag{2.35}$$

$$k_{P_2,(2)} = \sqrt{8D_{P(l)}v/\pi.r} \tag{2.36}$$

Where $D_{P(l)}$ is the phosphorus diffusion coefficient in molten silicon, v is the velocity of streamline flow, and r is the radius of the circular melt surface.

$$k_{P,(3)} = \frac{100\alpha p_P^* f_p}{\rho_{Si}} \sqrt{\frac{M_P}{2\pi RT}} \tag{2.37}$$

$$k_{P_2,(3)} = \frac{100\alpha p_{P_2}^* f_P^2}{\rho_{Si}} \sqrt{\frac{M_{P_2}}{2\pi RT}} \tag{2.38}$$

Where α is the surface evaporation coefficient.

$$k_{P,(4)} = \frac{D_{P(g)}}{\delta} \cdot \frac{\zeta_P}{e^{\zeta_P} - 1} \tag{2.39}$$

$$k_{P_2,(4)} = \frac{D_{P_2(g)}}{\delta} \cdot \frac{\zeta_{P_2}}{e^{\zeta_{P_2}} - 1} \tag{2.40}$$

Where $D_{P(g)}$ is the molecular diffusion coefficient of phosphorus, δ is the distance from the melt surface to the condensation surface, ξ_i is the diffusion effect factor of silicon vapour on phosphorus gas species i (i=P, P_2).

$$k'_{P,(4)} = \frac{100\, p_P^* f_P M_P}{RT\rho_{Si}} k_{P,(4)} \tag{2.41}$$

$$k'_{P_2,(4)} = \frac{100\, p_{P_2}^* f_P M_{P_2}}{RT\rho_{Si}} k_{P_2,(4)} \tag{2.42}$$

CHAPTER 3

EXPERIMENTAL PROCEDURE

3.1 Experimental Materials

Approximately 6kg of high purity crushed polysilicon was made available for the experiments. Iron and phosphorus had to be sourced and added to the polysilicon to the desired levels which are in the same range as those found in metallurgical grade silicon. A high purity pulverised iron metal was sourced for use in the experiments. A milled silicon phosphorus alloy was also procured for the experiments, the first batch of the silicon phosphorus alloy was consumed to completion during the experiments, and a different batch was subsequently used in the testwork. Crushed metallurgical grade silicon was sourced from a local supplier to be used in some of the experiments. Argon gas with a purity of 99.999% was used to provide an inert atmosphere during the experiments. The chemical analysis of the samples used for the testwork is presented in the table below.

Table 5 Chemical analysis of raw materials detailing elements of interest

Material	Si (%)	Fe(ppm)	P(ppm)
Polysilicon	matrix	-	-
Si-P alloy (1)	matrix	196	314.1
Si-P alloy (2)	matrix	210	440
Fe		995000	-
MG-Si	99	5000	16.5

No prior preparation was necessary for the materials used in the testwork. This was an advantage as possibilities for contamination were minimised. The raw materials used are shown in the figures below.

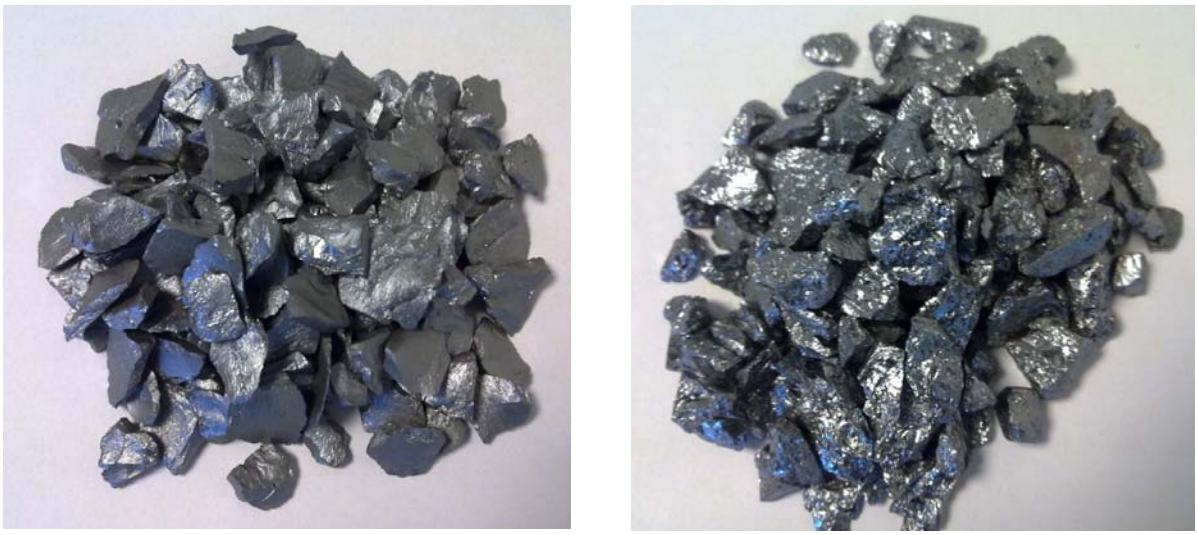

Figure 9: Main silicon sources for the experiments: polysilicon (left), metallurgical grade silicon (right)

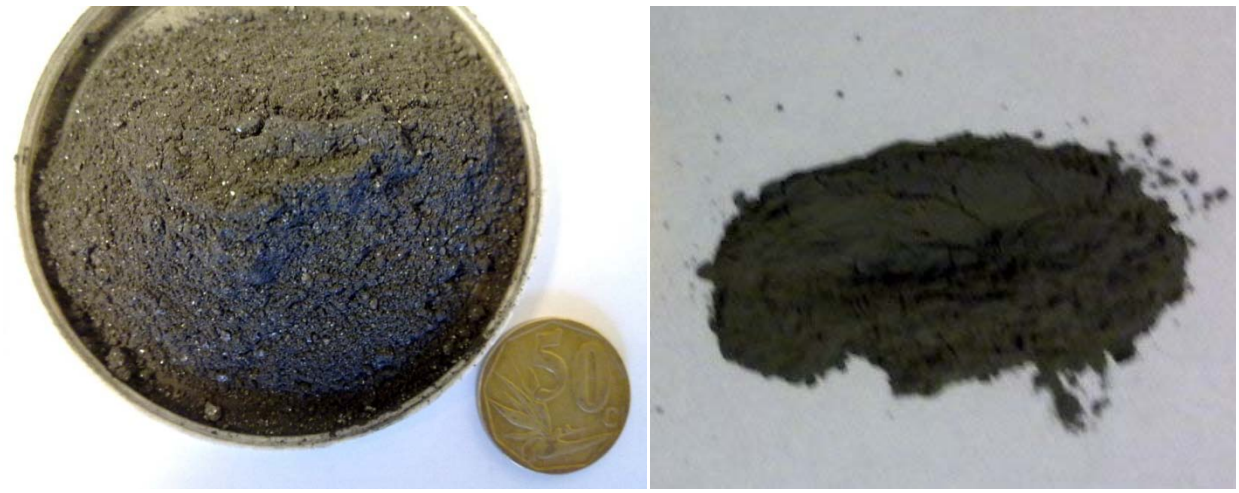

Figure 10: Major impurity sources for the experiments: Si-P alloy (left), iron (right)

3.2 Equipment description

3.2.1 Overview

The vacuum refining testwork was conducted in a vacuum induction furnace (Blue induction furnace) in a laboratory at the Department of Materials science and Engineering at NTNU. The set-up comprised of the vacuum chamber, control panel, power supply, water cooling circuit and a gas system. A general view of the vacuum induction furnace is shown in Figure 11 and a schematic diagram of the facility is shown in Figure 12.

Figure 11: General view of the vacuum induction furnace facility set-up

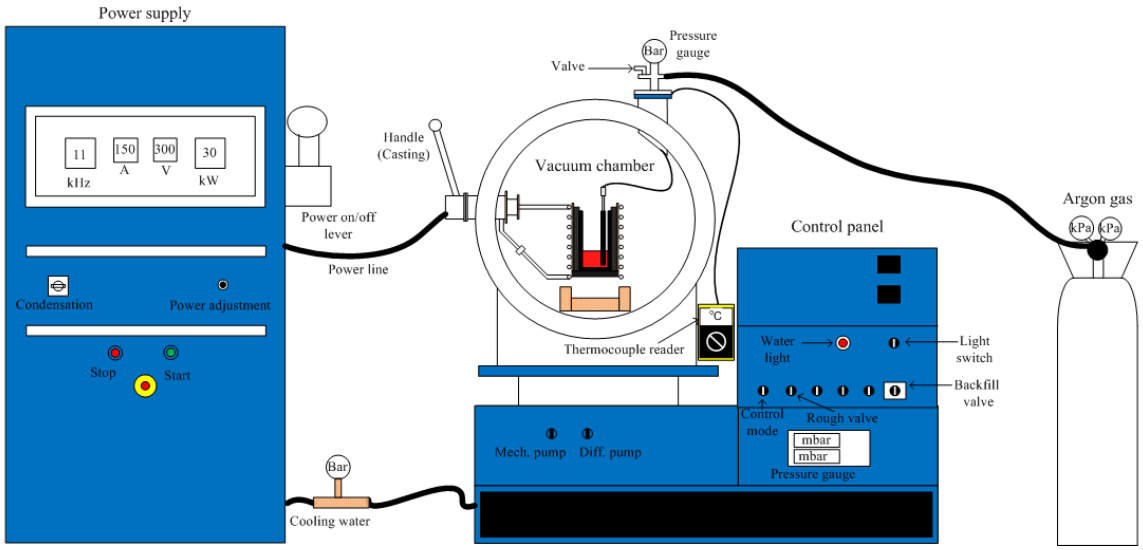

Figure 12: Schematic diagram of the experimental facility set-up

3.2.2 Vacuum chamber

The vacuum chamber comprised a cylindrical tube (OD = 0.59 m, ID = 0.5 m, l = 0.75 m), water-cooled induction coil and a water cooled copper casting plate. There are a number of valves and flow meters in place to control the pressure, and monitor the gas flow-rates into the vacuum chamber. For each experiment the sample containing crucible was wrapped with carbon wool and mica sheet and would then be inserted into the water-cooled induction coil. A C-type thermocouple was then placed in the crucible and connected to the thermocouple

chord which was in turn connected to the thermocouple reader. The vacuum chamber is shown in Figure 13 and the schematic of the vacuum chamber is shown in Figure 14

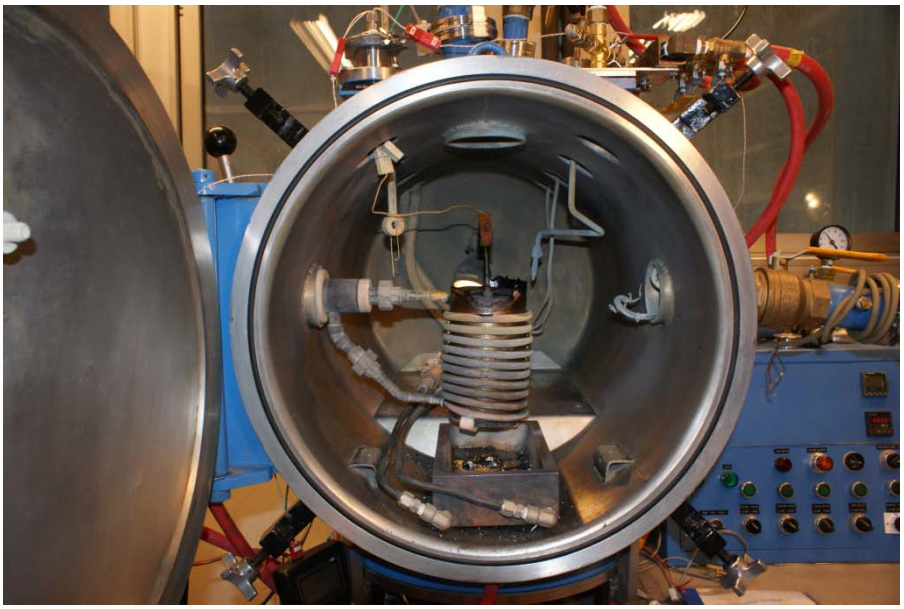

Figure 13: Diagram of the vacuum chamber with a crucible in place

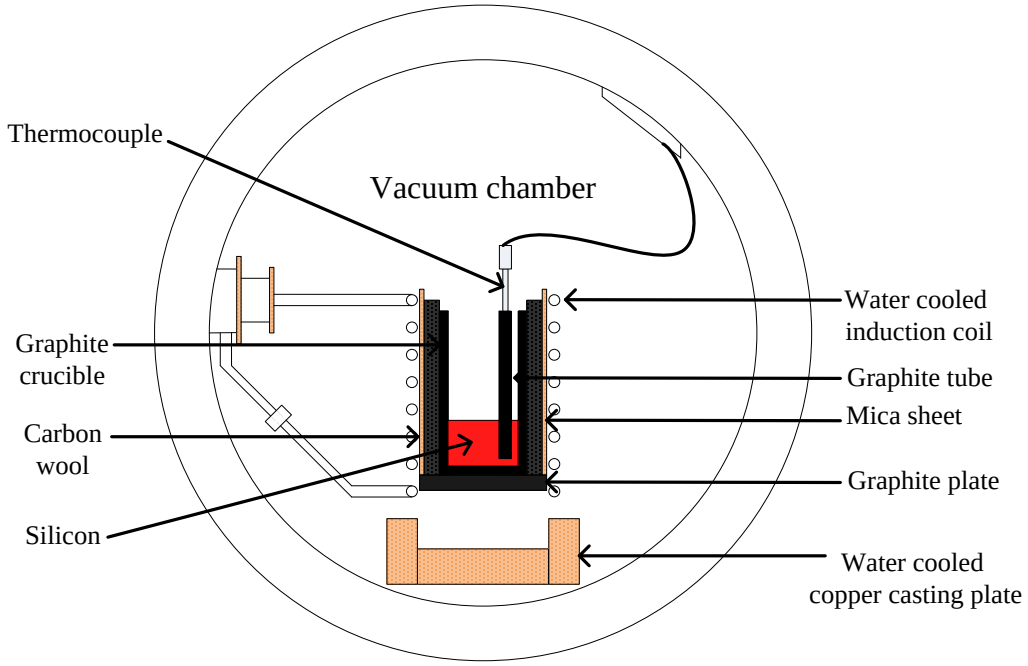

Figure 14: Schematic diagram of the vacuum chamber with a crucible in place

3.2.3 Water-cooling circuit

The power supply and some of the components of the vacuum chamber were water cooled. It was essential that water cooling was switched on for the duration of the experiments.

3.2.4 Gas purging

A cylinder of argon gas was connected to the vacuum chamber through tubes, valves and flow rate monitors. The main objective of this arrangement was to ensure that the vacuum chamber is operated under an inert atmosphere.

3.3 Experimental conditions and procedure

A total of 24 experiments were carried out of which 1 was unsuccessful, and the remainder of this thesis will focus on the 23 successful experiments. The same procedure was applied to all the experiments that were carried out. The experimental procedure for the experiments is detailed below.

1. Recipe preparation i.e. weigh polysilicon, silicon phosphorus alloy and Iron, and place in the graphite crucible (ID = 0.064 m, height of melted material = 0.04 m). Note: for metallurgical-grade silicon experiment, the recipe comprised metallurgical-grade silicon. Moreover, there were no iron additions in some of the experiments. Recipe mass was 300g for all the experiments.
2. Prepare the crucible for vacuum chamber: the crucible with contents was covered with a layer of carbon wool on the sides and at the botton, and covered with mica sheet on the sides.
3. Place the prepared crucible into the slot within the water-cooled induction coil in the vacuum chamber. Clean the vacuum chamber thoroughly prior to placing a crucible.
4. Insert a thermocouple in the graphite rod fixed in the crucible, and connect the thermocouple reader to the thermocouple using the compensation cable. C-type thermocouples were used on all the experiments.
5. Close the vacuum chamber with its contents and switch the mechanical pump on, and open the mechanical pump valve.

   The pressure in the vacuum chamber will now decrease automatically to very low pressures (less than 0.13 Pa)
6. After about 2 hours of vacuum operation, close the mechanical pump valve and open the inlet gas line, adjust the flow rate of argon accordingly.

   The pressure will now increase in the vacuum chamber.
7. Once the pressure reader reaches 0.5bar, close the inert gas line and open the mechanical pump valve to establish low pressures in the vacuum chamber.

8. Repeat step 6 and step 7 once to ensure an inert atmosphere in the vacuum chamber.
9. After about 18 hours of vacuum operation open water valve. The low water light will now turn off.
   The furnace power can now be switched on.
10. Move power lever to position 1 on the power panel.
11. Press the start button on the power panel.
12. Increase the power set-point to 2kW.
    Heat the crucible to a temperature of 500^{o}C at this power setting.
13. On reaching 500^{o}C increase the power set-point to 5kW.
    Heat the crucible to the desired temperature.
14. Once the desired temperature is reached, adjust the power accordingly to maintain the desired temperature (1500±5^{o}C, or 1600±5^{o}C) for the duration of the experiment (0min, 30min, 60min or 120 min).
15. If the vacuum pressure is below 10Pa, when the desired temperature is reached, then start counting the vacuum refining time. If not, wait until the pressure is 10Pa before start counting the vacuum refining time. One the vacuum pressure is at 0.5Pa or below start controlling the pressure by opening and closing the mechanical pump valve, desired pressure (0.5±0.2Pa).
16. At the conclusion of each experiment, cast the crucible material onto the water cooled copper casting metal.
17. Switch the power off.
18. Power lever to position 0 on the power panel.
19. Close the mechanical pump valve.
20. Switch the mechanical pump off.
21. Once the temperature in the vacuum chamber is deemed low to handle the material, open the pressure valve on the vacuum chamber to take the vacuum chamber out of vacuum.
22. Open the lid of the vacuum chamber, and place the sample in a labelled plastic bag for sample preparation.
    Sample preparation will be detailed under the characterisation section.
23. Close the water valve
24. Clean the vacuum chamber for the new experiment.

The different recipes that were prepared for the experiments are summarised in Table 6, and the details of the 23 experiments that were carried out are summarised in Table 7 below.

Table 6 Recipes prepared in a graphite crucible for the experiments

Polysilicon (g)	Si-P alloy (g)	Fe metal (g)	MG-Si (g)	Total (g)
280.9	19.1	0.146	-	300
279.4	19.1	1.496	-	300
280.3	19.1	0.598	-	300
285.8	13.6	0.598	-	300
286.4	13.6	-	-	300
-	-	-	300	300

Table 7 Summary of the experiments detailing concentration, temperature and time

	Concentration		1500°C			1600°C			
Si (%)	P (ppm)	Fe (ppm)	30 min	60 min	120 min	0 min	30 min	60 min	120 min
matrix	20	500	+	+		+	+	+	
matrix	20	2000	+	+	+	+	+	+	+
matrix	20	5000	+	+		+	+	+	
matrix	20	0	+	+		+	+	+	
98				+					

3.4 Characterisation

The different analytical techniques used to further characterise the samples are given in this section. Moreover, sample preparation was necessary prior to analysis; such procedures are also detailed in this section. ICP-MS served as the primary analytical technique and all the samples were analysed using ICP-MS for all the elements of interest. The 4-point resistivity method was also used to analyse the samples, and only phosphorus could be analysed via this technique. Lastly, GDMS was used to analyse a few samples.

3.4.1 ICP-MS

3.4.1.1 Sample preparation

The casted samples had to be milled prior to ICP-MS analysis. The pulverising was conducted in a Herzog vibration grinding mill. A tungsten carbide grinder head was used. This particular grinder head was selected on the premise that it only contaminated the samples with elements that are of no interest to this project work i.e. tungsten, carbon and cobalt. This was confirmed

on the work carried out by the author of this thesis prior to undertaking this project. Sample mass was approximately 20g for all the samples and each grinding cycle was 30 seconds. In between grinding cycles of experimental samples, polysilicon was milled to avoid contamination of one sample from previous grinding cycles. Sufficiently fine samples adequate for ICP-MS were produced. No particle size distribution was taken for the samples. The grinding equipment is shown in the figure below.

Figure 15: Grinding equipment: grinding mill (left), tungsten carbide grinding head (right)

3.4.1.2 ICP-MS analyses

The ICP-MS analysis was performed at the laboratory of NTNU. The ICP-MS instrument is a high resolution ELEMENT 2 from Thermo Electronics. All the elements of interest in the samples were analysed via ICP-MS, the most important elements included P, Fe and Si. Other elements that were analysed are as follows: Al, B, Ca, Co, Cu, K Mg, Mn, Na, Ni, Ti, V and W. A maximum of 45mg of each milled sample was weighed and placed in a Teflon bottle. The samples had to be digested and dissolved prior to chemical analysis. Hydrogen fluoride and nitric acid were used for the digestion of the samples. The samples were subsequently

dissolved at 80^{o}C for an hour with ultrasonic bath. The samples were then diluted to a final volume of 216ml. The samples were analysed in the ICP-MS instrument operating with argon methane plasma.

3.4.2 Resistivity analysis (Four points probe resistivity measurement) and GDMS

3.4.2.1 Sample preparation

The casted sampled were grinded to a mesh size of 500 in a twin wheel grinding/polishing machine using silicon carbide papers. This was done to produce a smooth surface on the samples for resistivity measurements. The same samples were used for GDMS analysis.

3.4.2.2 Resistivity analyses

The resistivity analysis was performed at a laboratory at NTNU. The instrument is a multiposition wafer probe from Jandel Engineering Limited. Resistivity of the samples were measured, these were converted to dopant density, and to dopant concentration. Only phosphorus could be analysed from the samples by this method.

3.4.2.3 GDMS analyses

GDMS analysis was performed at a laboratory at NTNU. The instrument is a. The samples from the first seven experiments were analysed via GDMS as a cross check as to whether removal of phosphorus was achieved or not from the experiments. The following elements were analysed via GDMS: Cu, Fe, P and Si.

CHAPTER 4

RESULTS

4.1 Analytical Results

As mentioned previously, three different analytical techniques were employed to analyse the samples for evaluating the refining process and for characterisation. Phosphorus was the most important element to be analysed, and it was analysed by all the three analytical techniques, namely IC-MS, GDMS and resistivity analysis. As mentioned in the previous chapter, GDMS technique was used for analysis of iron and copper and silicon. The ICP-MS technique was used to analyse for the elements deemed of interest for the testwork as outlined in the previous chapter.

4.1.1 Phosphorus analyses

Table 8 shows phosphorus analysis for all the samples subsequent to refining employing the different analytical techniques under the different refining conditions.

Table 8 Chemical assays of the experimental samples for phosphorus employing different analytical techniques

	Experiment description					Chemical assays, ppmw		
Experiment	Si (%)	P (ppmw)	Fe (ppmw)	temperature (K)	holding time (s)	ICP-MS	Resistivity	GDMS
1	matrix	20	500	1873	3600	7.5	2.9	6.9
2	matrix	20	500	1873	1800	11.8	7.6	9.6
3	matrix	20	500	1773	1800	14.6	9.0	9.9
4	matrix	20	500	1873	0	16.4	13.3	8.5
5	matrix	20	500	1773	3600	12.6	5.5	8.5
6	matrix	20	5000	1873	0	15.0	8.5	7.6
7	matrix	20	5000	1873	1800	13.0	7.9	4.9
8	matrix	20	5000	1873	3600	8.7	4.6	4.0
9	matrix	20	5000	1773	1800	14.7	5.8	8.5
10	matrix	20	5000	1773	3600	13.0	10.3	10.0
11	matrix	20	2000	1873	0	14.5	9.5	7.3
12	matrix	20	2000	1773	1800	14.1	5.9	8.9
13	matrix	20	2000	1773	3600	13.1	6.2	9.0
14	matrix	20	2000	1873	1800	10.9	3.2	6.8
15	matrix	20	2000	1873	3600	6.5	3.4	4.3
16	matrix	20	2000	1773	7200	9.2	2.5	-
17	matrix	20	2000	1873	7200	1.5	1.3	-
18	matrix	20	0	1873	0	14.4	4.6	-
19	matrix	20	0	1873	1800	9.5	3.6	-
20	matrix	20	0	1873	3600	6.6	2.2	-
21	98	17	5000	1773	3600	11.2	108.7	-
22	matrix	20	0	1773	1800	10.0	2.0	-
23	matrix	20	0	1773	3600	11.0	4.4	-

The phosphorus assays from all the different analytical techniques show that phosphorus removal was achieved on all the experiments since the reported phosphorus content subsequent to each experiment was less than the original phosphorus content. The overall trend for the phosphorus removal was decreasing phosphorus content with increase in temperature and holding time. The highest phosphorus removal was achieved after refining at 1873 K after a holding period of 7200 seconds and is reported to be 1.3 ppmw by the resistivity measurements, while the least phosphorus removal was achieved after refining at 1873 K at 0 seconds and is reported to be 16.4 ppmw by ICP-MS.

The phosphorus content measured by GDMS and resistivity measurements seem to be consistently lower than that measured by ICP-MS. The phosphorus assays under ICP-MS seem to be more consistent compared to assays from GDMS and resistivity measurements.

There seem to be some agreement between the different analytical techniques, this agreement is however minimal.

4.1.2 Iron analyses

Iron is an important impurity in metallurgical-grade silicon, and it was also of importance to the refining experiments as its effect on the removal of phosphorus was studied. The assays of iron content prior to each experiment versus the iron content subsequent to each experiment are shown in Table 9.

Table 9 Iron chemical composition of the experimental samples employing different analytical techniques

	Original iron content	Iron chemical assays after refining, ppmw	
Experiment	Fe (ppmw)	ICP-MS	GDMS
1	500	277	83
2	500	390	158
3	500	351	168
4	500	423	68
5	500	410	23
6	5000	4938	39
7	5000	6550	24
8	5000	4987	58
9	5000	5470	388
10	5000	5465	1476
11	2000	1966	52
12	2000	2324	294
13	2000	1653	801
14	2000	2252	88
15	2000	2264	405
16	2000	2173	-
17	2000	2001	-
18	0	11	-
19	0		-
20	0		-
21	5000	4822	-
22	0		-
23	0		-

The experiments were divided into four different iron conditions as can be seen from Table 9. It must be noted that the original iron content was calculated based on blends of raw materials, and not on chemical analysis of the samples. The iron content in the samples after

refining experiments was within the same order of magnitude as the original iron content for ICP-MS assays, and much lower than the original iron content for GDMS analysis. The lower iron content observed for samples analysed via GDMS could be attributed to the segregation of iron during cooling, but this will not be explored further since segregation only takes place after the vacuum refining process and therefore has no impact on the removal of phosphorus from silicon via the vacuum refining process.

CHAPTER 5

DISCUSSION

5.1 Vacuum refining characterisation results

The chemical analysis of samples from the refining testwork is presented in chapter four of this report. On the basis of consistency achieved with ICP-MS analysis as discussed in chapter four, all the chemical analysis used in this chapter will be based on ICP-MS results. To benchmark the refining testwork, the obtained analytical results will be compared to those achieved by other researchers who have published results from vacuum removal of phosphorus from silicon. Figure 16 shows concentrations of phosphorus as a function of time for different iron concentrations.

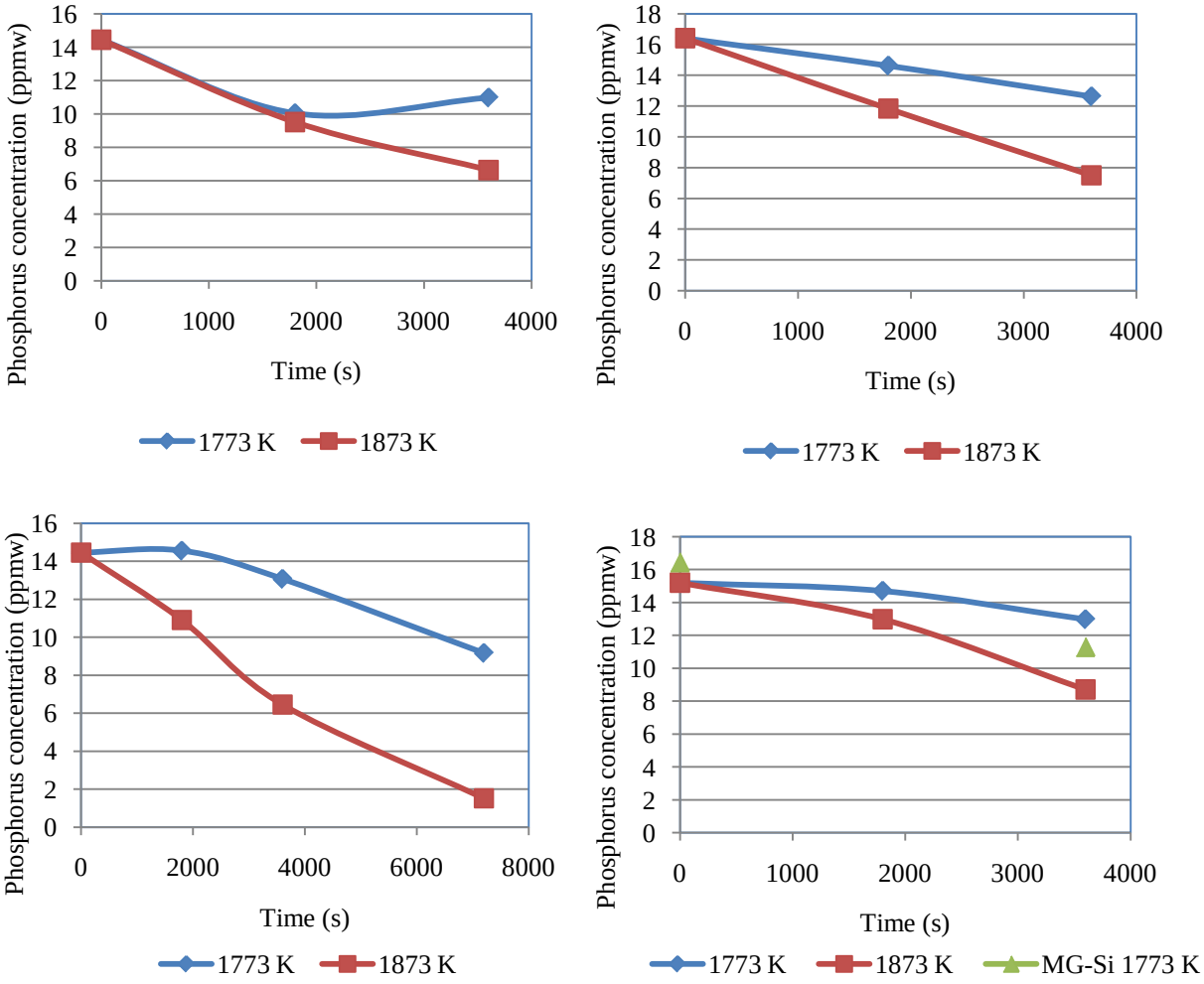

Figure 16: Phosphorus concentration as a function of refining time at different temperatures and iron concentrations: 0 ppmw (top left), 500 ppmw(top right), 2000 ppmw (bottom left), 5000 ppmw (bottom right).

The figure above shows that removal of phosphorus from silicon melts was achieved for all the different iron concentrations as the phosphorus concentration decreases with time. The highest phosphorus removal was achieved under both high temperature and maximum holding time which is in agreement with literature [34]. The initial concentrations show a variation between 14.5 ppmw and 16.5 ppmw, which could be attributed to inconsistencies between the different experiments. For consistency a staring concentration of 15.5 ppmw would be used for subsequent evaluation of the results. The phosphorus concentration for the metallurgical grade silicon experiment is slightly lower in comparison to that of the high purity silicon experiment; this could be attributed to the fact that the starting concentration of the metallurgical grade silicon was 16.4 ppmw as opposed to 20 ppmw for the high purity silicon. It can therefore be deduced that the nature of phosphorus removal from high purity silicon is somewhat comparable to that achieved from metallurgical grade silicon.

Figure 16 also shows that the phosphorus concentrations at 1773 K are consistently lower than those reported at 1873 K which is consistent with literature [34]. The phosphorus removal from the results given in Figure 16 seems comparable to the literature values reported in section 2.1.1.

5.2 Evaporation Kinetics

The evaluation of the absolute concentrations of phosphorus with time is not sufficient to fully describe the refining process. It is necessary to evaluate the relative concentrations and obtain the rate constants which can be compared to values reported in literature. Since the initial phosphorus concentration in silicon for the experiments is below 64 ppmw, it can be assumed that the refining of phosphorus from the silicon melt follows equation 2.12 as follows:

$\underline{P}$ (mass %, in Si) = P (g) (2.12)

The kinetics can therefore be described by equation 2.25 as shown below:

$$\frac{d[mass\%P]_1}{dt} = -\frac{A}{V}k_p[mass\%P] \quad (2.25)$$

Note:

$$mass\%P = C_{\underline{P}} \tag{5.1}$$

Integration of equation (2.25) renders the following equation:

$$LnC_{\underline{P}} / C_{\underline{P_o}} = -k_{\underline{P}}(A/V)t \tag{5.2}$$

Moreover, it would be assumed that the removal rate of phosphorus from silicon is controlled by the chemical evaporation reaction at the melt-gas interfacial area, and this assumption would be evaluated further at a later stage in this chapter. Figure 17 shows plots of $Ln(C_{\underline{p}}/C_{\underline{po}})$ versus (A/V)t for different iron concentrations where the mass transfer coefficient can be calculated from the slopes. A/V for the experiments is 25/m based on the crucible dimensions and molten silicon in the crucible

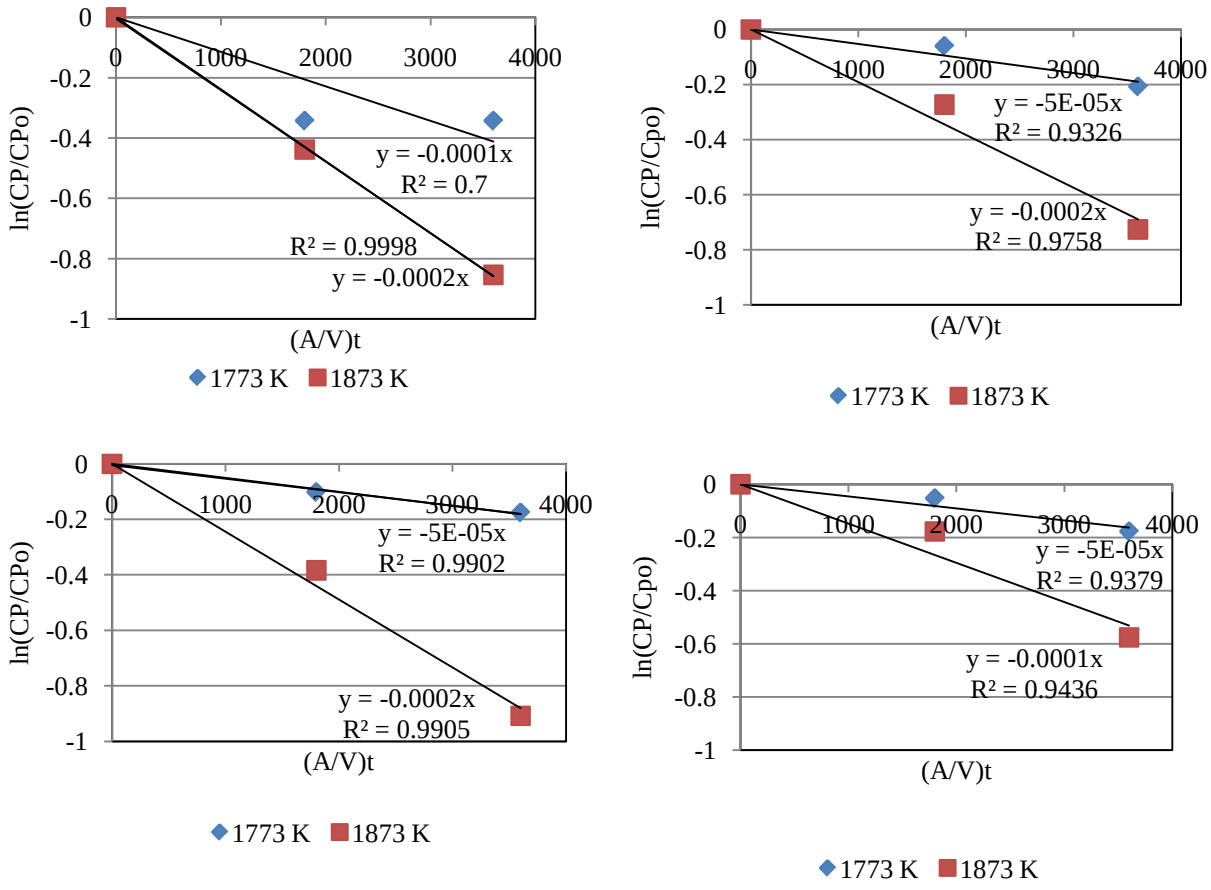

Figure 17: Plot of $ln(C_{\underline{P}}/C_{\underline{P_o}})$ versus (A/V)t for phosphorus at different temperatures and iron concentrations: 0 ppmw (top left), 500 ppmw(top right), 2000 ppmw (bottom left), 5000 ppmw (bottom right).

The plots obtained in Figure 17 show a linear relationship which indicates an agreement between the experimental results and the first order kinetics as described by equation 5.2. This therefore confirms literature predictions that P(g). is the predominant gas species at low phosphorus concentrations in silicon. [24,[33] The slopes of the plots are shown in the figure above and these are the mass transfer coefficients. For iron concentrations of 500 ppmw to 5000 ppmw mass transfer coefficients are approximately $2x10^{-6}$m/s at a temperature of 1773 K. Moreover, the mass transfer coefficients for iron concentrations between 0 ppmw and 2000 ppmw are approximately $1x10^{-5}$m/s.

Figure 18 shows the mass transfer coefficients as a function of iron concentration at 1773 K and 1873 K.

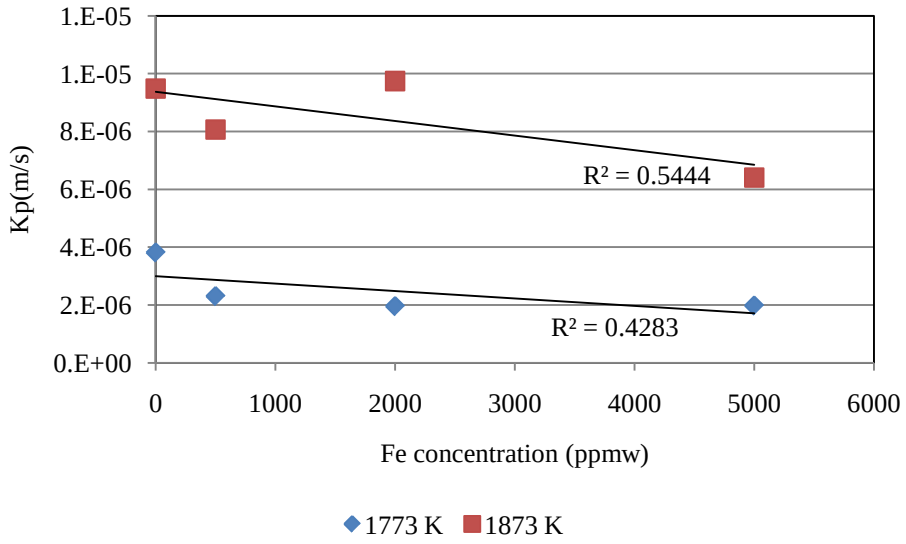

Figure 18: Mass transfer coefficients as a function of Fe concentration

As can be seen from the plot above the mass transfer coefficients show no correlation with iron concentration. Based on this plot as well as Figure 17 iron seems to have no effect on the removal of phosphorus from high purity silicon under the evaluated experimental conditions. Average mass transfer coefficients based on Figure 16 and Figure 17 at 1773 K and 1873 K are $2.5x10^{-6}$m/s and $8.4x10^{-6}$m/s respectively. The obtained rate constants compare well with the values of $3.01x10^{-6}$m/s and $7.82x10^{-6}$m/s at 1773 K and 1873 K respectively reported by Luyima [22]. Moreover, Safarian and Tangstad [23] reported a rate constant of $1.87x10^{-6}$m/s at 1773 K which compares well with the $2.5x10^{-6}$m/s obtained in the current investigation.

5.3 Industrial relevance

The metallurgical route for the production of solar-grade silicon is gaining momentum in industry. As was discussed in chapter 1 of this thesis, the metallurgical route employs a number of different refining steps to refine specific impurities in each step. For optimal removal of the impurities it is therefore invaluable to understand the impact of one impurity on the removal of another impurity in the refining of metallurgical grade-silicon to solar-grade silicon. Such an understanding could lead to optimised flowsheets for refining of metallurgical-grade silicon to solar-grade silicon.

The main finding of this testwork, which is that iron seems to have no effect on the removal of phosphorus from silicon melts is important industrially, in that the refining scheme from metallurgical-grade silicon to solar-grade silicon can either be designed such that iron is removed prior to phosphorus removal, or that phosphorus can be removed prior to iron removal, and this would have minimal impact on the overall refining process.

Moreover, the experimental results showed that refining at temperatures of 1773 K was minimal in comparison to that achieved at 1873 K, and that long holding times prove to be advantageous in the removal of phosphorus from silicon. The experimental results showed that induction vacuum refining is a promising technique for the removal of phosphorus from silicon.

CHAPTER 6

CONCLUSIONS

Induction vacuum refining testwork for the removal of phosphorus from silicon melts was carried out successfully. The refining process was studied with emphasis on the effect of iron on phosphorus removal from silicon. The raw materials for the experiments comprised high purity silicon with additions of phosphorus and iron to render blends with a phosphorus content of approximately 20 ppmw, and different iron contents as follows: 0 ppmw, 500 ppmw, 2000 ppmw and 5000 ppmw. The investigated temperatures and pressure were as follows, 1773 K - 1873 K and 0.5± 0.2 Pa, respectively. Holding times at the temperature of interest varied between 0 s and 7200 s.

ICP-MS seemed to be the most consistent of the analytical techniques employed for chemical analysis. Chemical analysis via resistivity measurements was found promising for phosphorus analyses in high purity silicon melts.

The experimental results showed that the starting phosphorus content decreased from 20 ppmw to approximately 15.5 ppmw during melting. Moreover, the phosphorus content decreased to 1.5 ppmw after vacuum treatment at 1873 K and at a holding time of 7200 s. The removal of phosphorus was found to be substantial at 1873 K in comparison to that achieved at 1773 K. The removal of phosphorus from silicon via induction vacuum refining seems independent of iron concentration for the investigated iron concentrations. The rate constants for phosphorus removal were determined to be 8.4×10^{-6}m/s and 2.5×10^{-6}m/s at 1873 K and 1773 K respectively. The removal rate of phosphorus was found to follow a first order equation where the monatomic gas species P is the predominant phosphorus species in the gas phase. It was proposed that the overall removal rate of phosphorus from silicon melts is controlled by free evaporation from the silicon melt surface.

CHAPTER 7

REFERENCES

[1] A.F.B. Braga, S.P. Moreira, P.R Zamperi, J.M.G. Bacchin, P.R. Mei. New processes for the production of solar-grade polycrystalline silicon: A review. *Solar energy materials and solar cells*, volume 92, issue 4, 2008: 418-424

[2] Green, M.A., Crystalline and thin film silicon solar cells: state of the art and future potential, *Solar energy materials and solar cells*, 2003, 74, 181-192.

[3] Hoffmann, W., PV solar electricity industry: market growth and perspective, *Solar energy materials and solar cells*, 2006, 90, 18-19, 3285-.

[4] Global market outlook for photovoltaics until 2014, EPIA, January 2011. http://www.epia.org/fileadmin/EPIA_docs/public/Global_Market_Outlook_for_Photovoltaics_until_2014.pdf

[5] Zhang, L., Ciftja, A., Recycling of solar cell silicon scrap through filtration, Part 1: experimental investigation, *Solar energy materials and solar cells*, 2008, 92, 1450-1461.

[6] Di Sabatino, M., Binetti, S., Libal, J., Acciarri, M., Nordmark, H., Øvrelid, E. J., Oxygen distribution on a multicrystalline silicon ingot grown from upgraded metallurgical grade silicon, *Solar energy materials and solar cells*, 2011, 95, 529-533.

[7] Sarti, D., Einhaus, R., Silicon feedstock for the multi-crystalline photovoltaic industry, *Solar energy materials and solar cells*, 2002, 72, 27-40.

[8] Goetzberger, A., Hebling, C., Schock, H. W., Photovoltaic materials, history, status and outlook, *Materials science and engineering*, 2003, R.40, 1-46.

[9] Murray, J. P., Flamant, G., Roos, C. J., Silicon and solar grade silicon production by dissolution of Si_3N_4, *Solar energy*, 2006, 80, 1349-1354.

[10] Woditsch, P., Koch, W., Solar grade silicon feedstock supply for PV industry, *Solar energy materials and solar cells*, 2002,72, 11-26.

[11] Pizzini, S., Towards solar grade silicon: Challenges and benefits for low cost photovoltaics, *Solar energy materials and solar cells*, 2010, 94, 1528-1533.

[12] Schei, A., Tuset, J., Tveit, H., Production of high silicon alloys, *Tapir Forlag*, Trondheim, 1998.

[13] Globe specialty metals products – silicon, January 2011.

http://www.glbsm.com/silicon-metal.aspx

[14] Möller, H, J., Funke, C., Lawrenz, A., Riedel, S., Werner, M., Oxygen and lattice distortions in multicrystalline silicon, *Solar energy materials and solar cells*, 2002, 72, 403-416.

[15] Green, M. A., Solar cells: Operating principles, technology and system applications, *Prentice-Hall*, Englewood cliffs, NJ, 1982, 122-123

[16] Lynch, D. C., Lynch, M. A., The search for a low cost solar-grade silicon, *Silicon for the chemical industry VII*, Norway, 2004, 21-24.

[17] REC group technology, January 2011.

http://www.recgroup.com/en/tech/FBR/

[18] Bartlett, J. E., Margolis, R. M., Jennings, C. E., The effects of the financial crisis on photovoltaics: an analysis of changes in market forecast from 2008 to 2009, *National renewable energy laboratory*, NREL Report no. TP-6A2-46713, 2009.

[19] Price, S., Margolis, R., Bartlett, J. E., 2008 solar technologies market report, Energy efficiency and renewable energy, *U.S. Department of energy*, 2010.

[20] Suzuki, K., Sakaguchi, K., Nakagiri, T., Sano, N., Gaseous removal of phosphorus and boron from molten silicon, *J. Japan Inst. Metals*, 1990, 54, 2, 161 -167.

[21] Yuge, N., Hanazawa, K., Nishikawa, K., Terashima, H., Removal of phosphorus, aluminium and calcium by evaporation refining in molten silicon, *J. Japan Inst. Metals*, 1997, 61, 10, 1086 -1093.

[22] Luyima, A., Removal of phosphorus from metallurgical grade silicon by the vacuum refining process, *Master's thesis*, Norwegian university of Science and technology, 2009.

[23] Safarian, J., Tangstad, M., Vacuum behaviour of the dissolved elements in molten silicon, *X. Silicon for the chemical industry*, 2010.

[24] Zheng, S., Safarian, J., Seongho, S., Sungwook, K., Tangstad, M., Luo, X., Elimination of phosphorus vaporizing from molten silicon at finite reduced pressure, *Transactions of nonferrous metals society of China. Metals*, 2011, 21, 697-702.

[25] Ikeda, T., Maeda, M., Purification of metallurgical silicon for solar-grade silicon by electron beam button melting, *J. ISIJ International*, 1992, 32, 5, 635 -642.

[26] Hanazawa, K., Yuge, N., Hiwasa, S., Kato, Y., Purification of metallurgical silicon for solar-grade silicon by electron beam button melting, *J. Japan Inst. Metals*, 2003, 67, 10, 569-574.

[27] Pires, J. C. S., Otubo, J., Braga, A. F. B., Mei, P. R., The purification of metallurgical-grade silicon by electron beam melting, *J. Journal of Materials Processing Technology*, 2005, 169, 1, 16-20.

[28] Miyake, M., Hiramatsu, T., Maeda, M., Removal of phosphorus and antimony in silicon by electron beam melting at low vacuum, *J. Japan Inst. Metals*, 2006, 70, 1, 43-46.

[29] Rosenqvist, T., Principles of extractive metallurgy, *Tapir Academic Press*, 2004.

[30] Harris., *Metallurgical Transactions B*, 1984, 15B, 251.

[31] Kubaschewski, O., Alcock, C. B., Metallurgical thermochemistry, *Pergamon Press*, 1979, 5th edition.

[32] Wei, K., Ma, W., Dai, Y., Yang, B., Liu, D., Wang, J., Vacuum distillation refining of metallurgical grade silicon (I) – Thermodynamics on removal of phosphorus from metallurgical grade silicon, *Trans. Nonferrous Met. Soc. China*, 2007, 17, 1022-1025.

[33] Miki, T., Morita, K., Sano, N., Thermodynamics of phosphorus in molten silicon, *J. Metallurgical and Materials Transactions*, 1997, 27B, 6, 937-941.

[34] Zheng, S., Engh, T. A., Tangstad, M., Luo, X., Numerical simulation of phosphorus removal from silicon by induction vacuum refining, *J. Metallurgical and Materials Transactions A*, 2011, DOI: 10.1007/s11661-011-0621-3.

[35] Ma, W., Wei, K., Yang, B., Liu, D., Dai, Y., Vacuum distillation refining of metallurgical grade silicon (II) – Kinetics on removal of phosphorus from metallurgical grade silicon, *Trans. Nonferrous Met. Soc. China*, 2007, 17, 1026-1029.